Journal of Volcanology and Geothermal Research 451 (2024) 108077

Contents lists available at ScienceDirect

Journal of Volcanology and Geothermal Research

journal homepage: www.journals.elsevier.com/journal-of-volcanology-and-geothermal-research

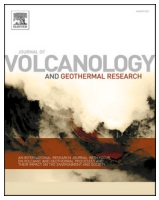

The 15 January 2022 Hunga (Tonga) eruption: A gas-driven climactic explosion

Richard W. Henley [a,*], Cornel E.J. de Ronde [b], Richard J. Arculus [c], Graham Hughes [d], Thanh-Son Pham [c], Ana S. Casas [c], Vasily Titov [e], Sharon L. Walker [e]

[a] ARC Training Centre for M3D Innovation, Research School of Physics, Australian National University, Canberra, ACT 2601, Australia
[b] GNS Science, Lower Hutt 5040, New Zealand
[c] Research School of Earth Sciences, Australian National University, Canberra, ACT 2601, Australia
[d] Faculty of Engineering, Department of Civil and Environmental Engineering, Imperial College London, SW7 2AZ, England
[e] NOAA Pacific Marine Environmental Laboratory (PMEL), Seattle, WA 98115, United States of America

ARTICLE INFO

Keywords:
Magmatic vapor
Gas-solid reaction
Hydraulic fracture
Atmospheric gravity waves
Meteotsunamis
Plinean eruption

ABSTRACT

An extraordinarily powerful, explosive eruption occurred from Hunga volcano in the Tonga island arc on 15 January 2022 and generated an eruption column 58 km high. The explosive eruption also generated atmospheric gravity waves, extreme runup tsunamis and quite unusual and destructive meteotsunamis. Together these place this VEI 6 eruption as, globally, one of the largest of the past 300 years.

Based on the oceanic context of Hunga volcano, it has previously been assumed that the eruption was phreatomagmatic through a fuel-coolant Surtseyan-type interaction, but this is not supported by satellite imagery. Similarly, it has been suggested that a caldera-collapse was the eruption trigger, but this is not supported by bathymetric data or the seismicity recorded during the eruption. Here we develop a new model based on the observed energetics and time sequence of the eruption integrated with understanding of the internal structure of active volcanoes and their characteristic high flux discharges of volcanic gas.

It has been shown elsewhere that magma-derived reactive gases (H_2O, CO_2, SO_2, HCl, etc) aggressively alter the volcanic rocks in the core of a volcano leading to self-sealing of gas flow to the surface and consequent changes to deviatoric stress in the structure. Common minerals developed by these reactions include anhydrite ($CaSO_4$), sulphides and silica (quartz), all of which have been recorded in volcanic ejecta including at Hunga.

We here develop a first order numerical model that quantifies how the free discharge of such gas to the surface may progressively become choked by these sealing reactions leading to increased internal gas pressure. Hydraulic fracture of the seal occurs when the transmitted pressure of the compressed magmatic gas beneath the seal increases to a value greater than the lithostatic pressure plus the tensile strength of the sealed rock. This initiates the explosive release of compressed gas whose high-power discharge progressively develops and enlarges a crater. At the same time, the explosion feeds upon itself by generating larger pressure gradients in the pressurized gas within the fractured porous rock mass of the core of the volcano. Excavation of the crater may intersect high level intrusions and produce the pumice rafts that were observed after the eruption. The eruption itself diminished in intensity as the gas pressure in the reservoir declined.

At Hunga, the eruption excavated an 850 m deep, 2-3 km diameter steep-walled crater. This volume may be assumed to approximate the volume of fractured porous rock (the control volume of the eruption) whose trapped gas was mined by the eruption until surrounding gas pressure was depleted. Our numerical model shows that the calculated potential energy of the trapped compressed gas matches the independent observations of the scale of the eruption. Sensor data have since shown that gas bubble flares continued for at least 6 months after the eruption indicating continued depletion of the gas reservoir of rocks surrounding the new crater. The systems-based, gas-driven model for the Hunga climactic eruption developed here also applies to Plinean-type eruptions on subaerial arc volcanoes such as at Pinatubo (Philippines) 1991.

* Corresponding author.
E-mail address: Richard.Henley@anu.edu.au (R.W. Henley).

https://doi.org/10.1016/j.jvolgeores.2024.108077
Received 20 December 2023; Received in revised form 12 April 2024; Accepted 19 April 2024
Available online 21 April 2024

Nomenclature

Following the 15 January 2022 eruption, publications have often tended to refer to the volcano as Hunga Tonga-Hunga Ha'apai (HT-HH). However, the vast bulk of the edifice is called Hunga whereas HT-HH refer to the small structures (islands) on the northern rim of the summit crater. It is both anthropocentric and illogical to continue to use the label HT-HH for this volcano.

The January 2022 Hunga eruption is frequently referred to as 'climactic' assuming the sense of very large. The definition of this term is, according to Oxford languages, 'acting as a culmination or resolution to a series of events; forming an exciting climax' as is appropriate for this eruption.

The terms vapor and gas, as commonly used, are synonymous. A vapor is a gas phase that is in equilibrium with a condensed phase (solid or liquid) but has the properties of a gas. We use the term magmatic vapor to refer to gas inside a volcano that has been released by a magmatic system during its evolution and we use the term volcanic gas for gas discharged from a volcano.

Crater v caldera. Publications about the Hunga eruption have tended to use the term caldera indiscriminately. Following (Lipman, 2000) we use the term crater which, by definition, refers to a geomorphic feature derived by loss of erupted material and the term caldera for demonstrable collapse features in volcanic systems.

1. Introduction

On 15 January 2022, the intra-oceanic Hunga volcano (known as Hunga Tonga-Hunga Haapai before the eruption; Fig. 1) exploded with devastating consequences for the Kingdom of Tonga (Tarumi and Yoshizawa, 2023). The eruption generated a volcanic plume, parts of which quickly reached 58 km into the atmosphere with most particulates dispersing in layers between 20 and 30 km above sea level (asl). The fragmental rock fraction collapsing from the plume was dispersed as relatively high speed, submarine volcaniclastic density currents around the volcano and caused major damage to telecommunication cables (Clare et al., 2023). The explosive eruption produced tsunami waves that devastated local Tonga shores, wreaked havoc around the Pacific and were recorded right around the globe. The initial tsunami amplitudes that devastated local Tonga islands have been estimated to exceed 100 m in the vicinity of the volcano (Heidarzadeh et al., 2022; Lynett et al., 2022; Pakoksung et al., 2022; Purkis et al., 2023). The complex mechanism of the tsunami generation, the details of which are still being investigated, likely involves multiple sources, including cavity formation and air-pressure waves. The explosive eruption also generated a major and complex atmospheric disturbance comprising a spectrum of acoustic gravity waves, including Lamb waves (Matoza et al., 2022), which generated meteotsunamis around the globe. Uniquely for a major eruption, the global monitoring of these wave data has provided an independent basis for estimating the magnitude of the explosive energy of the 2022 Hunga eruption (Horváth et al., 2023; Matoza et al., 2022; Wright et al., 2022) suggesting that this eruption was comparable in size to that of Krakatau in 1883, and possibly larger.

The immediate questions arising from the climactic eruption eruptive sequence on 15 January 2022 concern its energetics and triggering mechanism. The Hunga eruption consisted primarily of a sequence of explosive events over an initial 30-min period. This sequence followed major eruptive activity over several weeks prior to January 15th and was succeeded a few hours afterwards (Matoza et al., 2022; Zheng et al., 2023) by another major explosive event. *Explosions*, by definition, are the irreversible expansion of gas consequent on disturbance of some highly condensed energy source (Keller et al., 2014). Examples in the context of active volcanoes are phreatomagmatic eruptions caused by the rapid release of dissolved volatiles from shallow ascending magma (Scheu and Dingwell, 2022), and fuel-coolant eruptions caused by flash vaporization as water contacts lava (Zimanowski et al., 2015). However, all of these *syn*-magmatic mechanisms are constrained in scale through the specific mass of magma that is involved in a very short time interval, and the surface area exposed to heat transfer. By contrast, in this paper, we suggest that the scale of the acoustic-gravity wave energy recorded in the first 30 min of the Hunga eruption was a measure of the mass of gas that had been exsolved from the deep magmatic system and trapped within the volcano *prior to* the eruption by sealing of the near-surface rock mass as it fluxed through the volcano. This mass of compressed gas, was then explosively released to atmospheric pressure following hydraulic failure of the sealed regime. We provide supporting evidence for this explosion model from bathymetry and satellite imagery and incorporate data from ocean drilling of volcanoes elsewhere in the Tonga-Kermadec arc. We also include evidence of the extent of gas-solid reactions in the interiors of arc volcanoes that has been provided by mining of porphyry copper mineral deposits that formed within them (Henley and Berger, 2013).

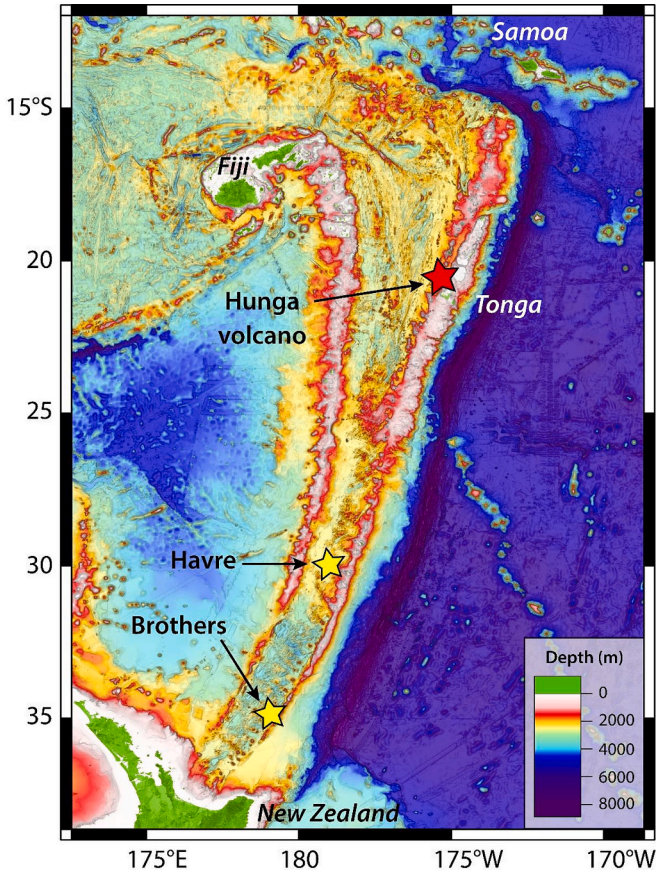

Fig. 1. Regional map showing locations of the Hunga (red star), Havre, and Brothers (yellow stars) submarine volcanoes in the southwest Pacific Ocean along the Tonga-Kermadec arc that strikes between New Zealand and the termination of the Tonga Trench south of Samoa. Hunga volcano (175.3841°W, 20.5532°S) is located within the Kingdom of Tonga. Base map was created using Global Multi-Resolution Topography Synthesis (GMRT; https://www.gmrt.org/GMRTMapTool/; geographic coordinate system is WGS84). (For interpretation of the references to colour in this figure legend, the reader is referred to the web version of this article.)

2. Data review and analysis

The independent sources of data that are available for an integrated analysis of the causes of the 15 January 2022 Hunga eruption include geological and bathymetric data that was accumulated pre- and post-eruption and a wide range of seismic, oceanographic and atmospheric data reported from global monitoring networks.

2.1. Geological setting

Hunga volcano is a ~ 200 km^3 largely submarine volcanic cone located 65 km NNW of Nuku'alofa, the capital of the Kingdom of Tonga on the island of Tongatapu (Fig. 1). The volcano is one of many predominantly submarine edifices defining the volcanic front of the Tonga-Kermadec arc (Beier et al., 2017). The Tonga arc is flanked 150 km to the east by the ~10,000 m-deep Tonga Trench, which marks the subduction locus of the Pacific Plate in this region (Bevis et al., 1995). The high subduction rate of the Pacific Plate, limited thickness and pelagic-hydrothermal nature of subducted sediment, and extensive submarine and subaerial volcanic activity are among the many features that have attracted multidisciplinary studies of plate convergence processes manifest in the Tonga-Kermadec arc and adjacent backarc systems (Conder and Wiens, 2006; Stoffers et al., 2006). Nevertheless, the detailed temporal history of the volcanoes is essentially unknown because sampling has been restricted to dredging, coring, and the limited exposures of subaerial outcrops. The petrogenesis of the active arc magmas is complex, with a variety of subducted plate inputs to mantle wedge sources that are variably depleted by prior partial melting (Cooper et al., 2010). Along the strike of the Tonga arc, tracers of subducted plate input to the genesis of arc magmas reach a peak at the latitude of Hunga volcano (Cooper et al., 2022). It is also appropriate to note that the prevailing stress state of the volcanic front edifices of the Tonga-Kermadec arc is extensional, as manifest by sub-arc parallel rifts (Caratori Tontini et al., 2019; Cooper et al., 2010).

Over the last 1000 years, Hunga volcano has experienced several major eruptions, the most recent at 1040–1180 CE (Zheng et al., 2023). Remnants of the evolved volcanic cone were preserved in the islands of Hunga Ha'apai and Hunga Tonga and shoals along the southern rim (Figs. 2 and 3). More recently, shallow submarine eruptions were observed in 1912, 1937, and 1988. Activity in 2009 began as submarine eruptions, progressing to subaerial as pyroclastic deposits added to the area of Hunga Ha'apai, but these deposits eroded away within ~6

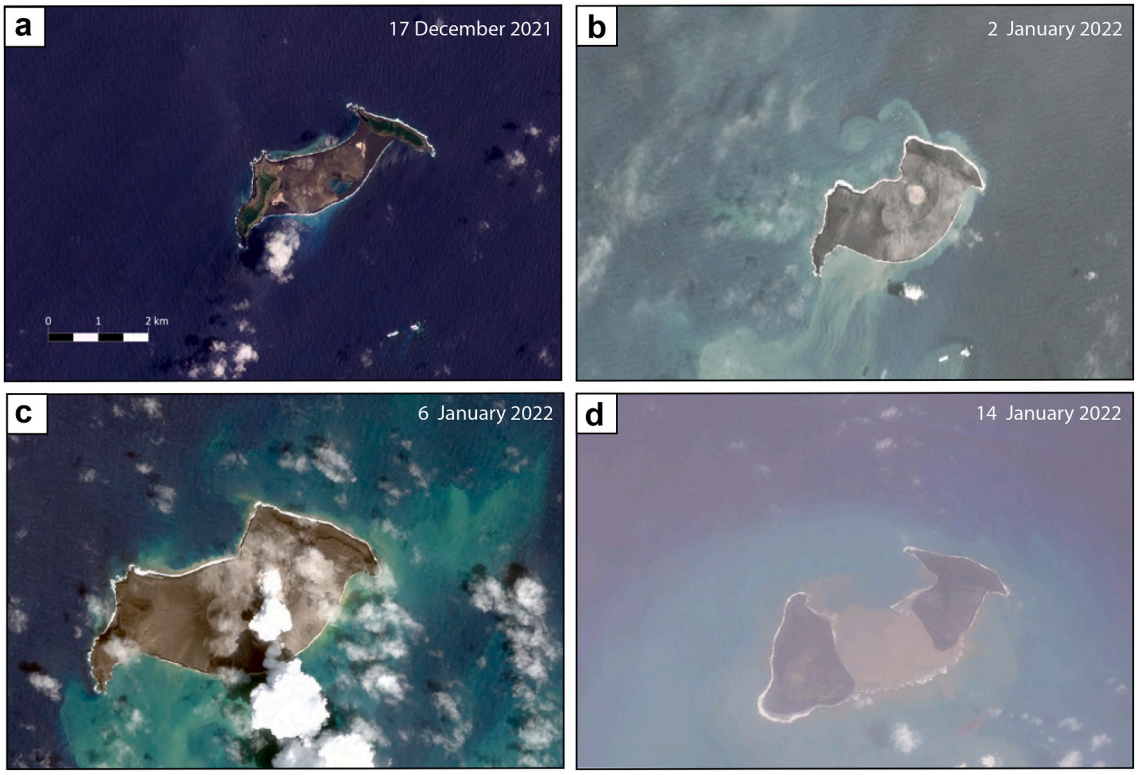

Fig. 2. Series of satellite photographs of Hunga Tonga-Hunga Ha'apai (i.e., the above sea level part of Hunga volcano) leading up to the main eruption of 15 January 2022 and presence of discolored seawater surrounding the island(s) that indicates ongoing degassing and hydrothermal fluid discharge. (a) Shows the state of the volcano on 17 December 2021, 7 days prior to the plume eruption of 24 December. The small volcanic cone, made of deposits from the 2014–2015 eruption, is active and contains a crater lake, persistent since 2015, that probably contains condensed volcanic gas. Distinct white areas around the base of the cone may be hydrothermally altered volcanic rocks, and discolored water near the shoreline is likely the result of hydrothermal fluid discharge through the flanks of the cone or direct outflow from the crater lake. (b) Shows the volcano on 2 January 2022 and the growth of the volcanic cone from deposits ejected during the eruptive phase that began 20 Dec 2021. The submarine fluid discharge continued while gas discharge from the cone was subdued. (c) Shows the volcano 6 January 2022 showing substantial on-going degassing principally from the volcanic cone and the crater lake that was well established. There was an increase in the extent of discolored seawater around the islands, and this is thought to represent the submarine discharge of 'magmatic-hydrothermal fluids' from the flanks of the cone. (d) Shows the quiescent state of the volcano one day prior to the climactic eruption. The above-sea level portion of the cone has been mostly removed but submarine fluid discharge continues. a. Image captured by Planet satellite on 17 December 2021 (20211217T210217_PS_2451_RGB_3m).
b. Image captured by Planet satellite on 2 January 2022 (20220102T212849_PS_1003_RGB_3m).
c. Image captured by MAXAR satellite on 6 January 2022 (20220106T215812_WV02_RGB_2m).
d. Image captured by Planet satellite on 14 January 2022 (20220114T210015_PS_2420_RGB_3m).
Scale bar shown for HT-HH in (a) can be used to scale all images.
All images accessed from the Hazards Data Distribution System (HDDS); all dates in UTC.

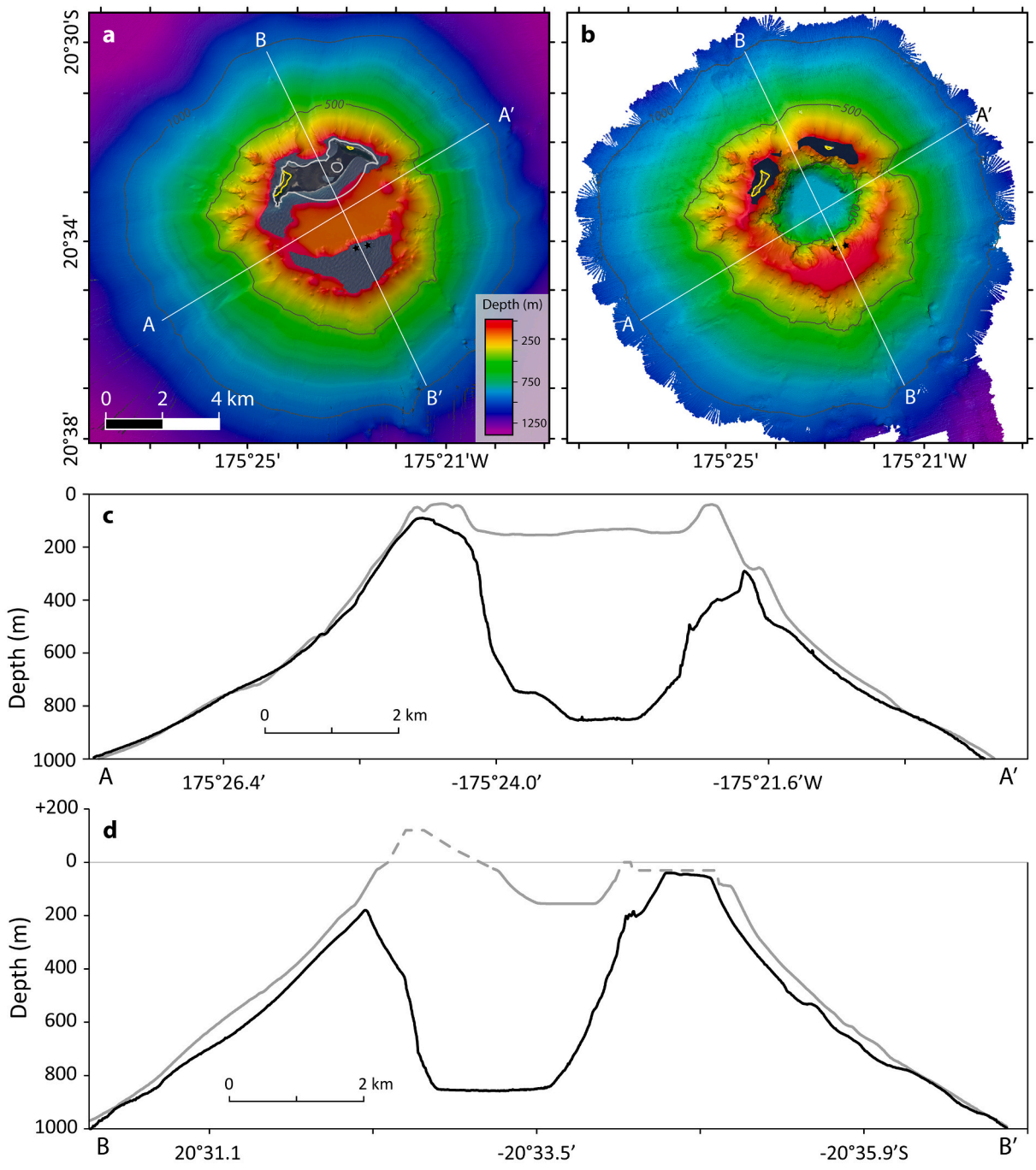

Fig. 3. Changes to the seafloor due to the explosive eruption on 15 January 2022: (a) pre-eruption (2016) bathymetry mapped by *R/V Falkor* during cruise FK160407 (Ferrini, 2022). White polygon outlines the extent of HT-HH island in early January 2022 (e.g., Fig. 2b) and its crater lake, which is outlined by the small white oval to the east of line B-B′. Depth colour scale and scale bar are the same for (b), white lines A-A' and B-B′ show locations of the depth profiles shown in (c) and (d), respectively; (b) post-eruption bathymetry mapped by USV *Maxlimer* in July/August 2022 DOI https://doi.org/10.5281/zenodo.10038897 see Supplementary Material (NIWA-Nippon Foundation TESMaP project, 2023) (c) depth profiles along line A-A' from 2016 (grey) and 2022 (black); (d) depth profiles along line B-B′ from 2016 (grey, dashed line estimates height of HTHH island built during 2015 eruption and south rim shoal that was too shallow for the R/V *Falkor* to map in 2016) and 2022 (black). Yellow polygons in (a) and (b) show remaining above-sea-level extent of the islands, post-eruption. (For interpretation of the references to colour in this figure legend, the reader is referred to the web version of this article.)

months (Global Volcanism Program, 2009). Eruptions in 2014/15 were also initially submarine prior to forming a persistent subaerial tombolo between the two islands (Brenna et al., 2022). The major explosive eruption of 15 January 2022 was preceded by several smaller eruptions between 19 December 2021 and 13 January 2022, which extended the tombolo between the islands toward the center of the crater region (see section 2.3.1 below).

2.2. Bathymetry and satellite imagery

The volcano's shape and profile pre- and post-2022 eruption, based on 2016 (Ferrini, 2022) and 2022 bathymetric grids (DOI https://doi.org/10.5281/zenodo.10038897 – see Supplementary Material) and satellite images (Fig. 2), are shown in Fig. 3. Relative to the 2016 bathymetric survey, the post-2022 eruption profile shows part of the

north-eastern rim is now missing and 6.3 km^3 of material has been removed from the center of the volcanic cone to produce an 850 m-deep, 2–3 km-diameter crater (see Supplementary Material). The new crater is sub-circular with a diameter of about 3 km at 200 mbsl (meters below sea level) and is conical in form, diminishing in diameter to about 1 km at a depth of 850 m. The form of the new crater appears to replicate the pre-existing surface topology observed in the 2016 survey. Within the crater, only minor scree slope formation is observed.

Our analysis of the volume of material removed in the 15 January 2022 Hunga eruption using the post-eruption bathymetry relative to the previous 2016 survey is given in the Supplementary Material. Satellite imagery taken immediately prior to the eruption (Fig. 2d) shows, at 10 m grid resolution, that at this time there was no surface volcanic activity, and that pyroclastic infill had been reduced to only a few metres below sea level between the two islands. Based on these and other observations, the volume of material lost during the formation of the new crater has been calculated to be 6.3 km^3. This volume provides a minimum estimate for the volume of pyroclastic materials ejected during the eruption, and a volcanic explosivity index (VEI) of 6 (Ringler et al., 2023). Our analysis also provides cross-sectional area data with 11.5 km^2 at the 200 mbsl contour diminishing through 8.4 km^2 at 400 mbsl, 5.8 km^2 at 600 mbsl to 2.9 km^2 at 800 mbsl.

2.3. Sequence of eruptive events and energy release

Review of published atmospheric, satellite and seismic data (Thompson et al., 2022) shows how intimately related these expressions of the climactic 15 January Hunga eruption were. Here, we summarise these data and integrate them with other key data sources such as post-eruption bathymetry, in order to derive a new understanding of the cause of the 15 January climactic eruption.

The 2022 Hunga eruption itself comprised several explosive events (Matoza et al., 2022), which were well-documented through the Comprehensive Nuclear-Test-Ban Treaty Organization (CTBTO). The eruption had been preceded by a sequence of recorded activities, including volcanic ash plume formation, over several weeks before the climactic eruption (Yuen et al., 2022; Zheng et al., 2023). The first observed activity in the new eruptive cycle that culminated on 15 January 2022, was noted at 20:46 UTC on 19 December 2021 and lasted until 4 January 2022 (Astafyeva et al., 2022). The volcano was then quiescent for about 9 days before resuming eruptive activity. An explosion at 15:20 UTC on 14 January developed an 18 km-high plume.

The climactic eruption sequence commenced at around 04:00 UTC on 15 January with a relatively small seismic event, interpreted as due to rock failure. This was followed by increased levels of background signals recorded by infrasound, seismic, barometric, lightning and hydroacoustic time series (Astafyeva et al., 2022; Le Bras et al., 2023; Matoza et al., 2022). At 04:10 a volcanic ash cloud had reached 18 km and spread to a 5 km radius (Thompson et al., 2022). Some of this initial activity disturbed the ionosphere (Astafyeva et al., 2022) and was heard by people in Nuku'alofa (Borrero et al., 2023; Purkis et al., 2023).

The principle earthquake and explosive events commenced at 04:15 UTC (Fig. 4) and continued for about six minutes. Teleseismic data at 15–50 s resolved four to five sub-explosions during the six minutes of the escalated seismic crisis (Thurin et al., 2022; Zheng et al., 2023). However, this group of seismic events was observed as a single atmospheric event in lower temporal resolution data such as ionospheric and barometric time series (Fig. 4). At 04:20 the ash cloud had reached 30 km and may have been due entirely to the 04:15 explosion (Thompson et al., 2022). The cloud reached 55 km at 04:28 coinciding with a maximum in Lamb wave transmission prior to entering a negative phase at about 04:37 (Thompson et al., 2022). The eruption crisis finally concluded around 08:31 UTC, four hours after the trigger event. Due to the absence of seismic stations proximal to Hunga volcano, all seismic records are at relatively low frequencies so it is not possible to fully resolve the presence of any high-frequency seismic content which could support the presence of hybrid volcanic tremors (McNutt, 2005).

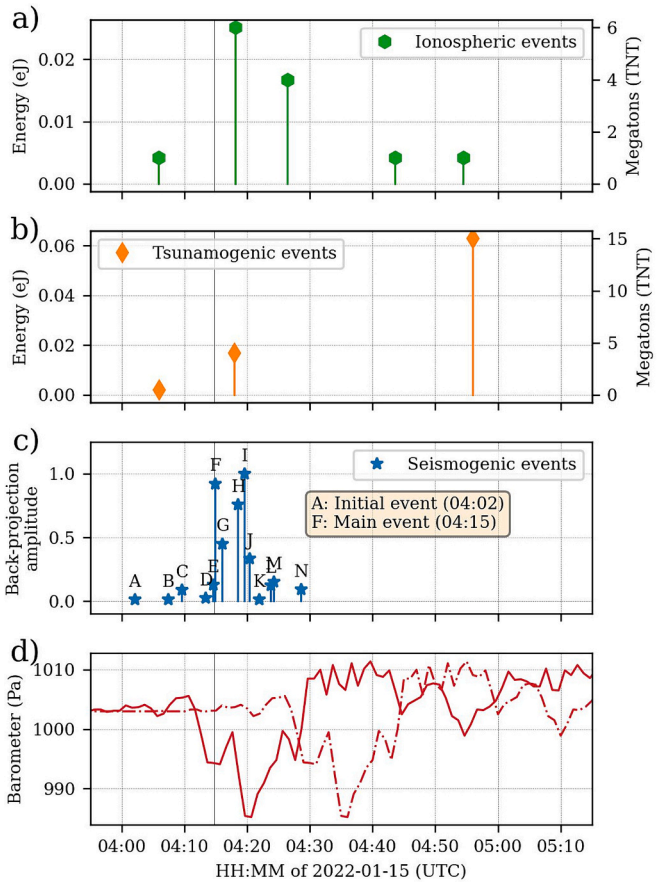

Fig. 4. Eruption sequence as inferred from (a) ionospheric (Astafyeva et al., 2022), (b) tsunamic (Purkis et al., 2023), (c) seismic (Tarumi and Yoshizawa, 2023), and (d) Tongan Met Office barometric data as reported by Purkis et al. (2023). In c, labels A to N designate identifiable seismic events. In (d), the dashed-dotted line shows the original barometric timeline while the solid line is advanced by 920 s to match the timelines of ground observations in other panels.

The generation of a spectrum of acoustic-gravity waves, recorded by the International Monitoring System and other entities, has provided the singular opportunity to attempt to constrain the energetics of the 15 January 2022 eruption of Hunga volcano. These data record the scale of the atmospheric disturbances due to the explosive sequence and immediately define the eruption as being at least similar in explosive energy to that of the 1883 eruption of Krakatau. We note, however, that there is a wide diversity of estimated eruptive energies for the 2022 eruption so that published values cannot be used directly (Matoza et al., 2022). Estimates based on seismic or tsunamic records (e.g., Donner et al. (2023), 0.4 EJ; Thurin et al. (2022), 0.001 EJ; Purkis et al. (2023), 0.06 EJ; Vergoz et al. (2022), 0.4–0.8 EJ; Yuen et al. (2022), ~0.2 EJ) are several orders of magnitude smaller than those estimated from Lamb or gravity-acoustic waves (e.g., Matoza et al. (2022), 20.8 EJ; Horváth et al. (2023), ~4.2 EJ ("of the order 1000 Mt $TNT_{equivalent}$"); Wright et al. (2022), 10–28 EJ; Kulichkov et al. (2022), 0.6 EJ; Díaz and Rigby (2022), 0.25 EJ), Astafyeva et al. (2022), 0.04–0.15EJ. In order to progress understanding of the explosion mechanism itself it is useful to benchmark its energy yield as >4 EJ. Importantly, these estimates, with the exceptions of Kulichkov et al. (2022), Díaz and Rigby (2022) and Astafyeva et al. (2022), may indicate that the quantum of energy released into the atmosphere by the eruption was substantially larger than the energy that was released into the solid Earth and ocean.

The energy intensity of the Hunga explosion has also been recorded

by the preservation of abundant damage cracks in ash particles and comparisons with particles from Krakatoa and Havre volcanoes (Baxter et al., 2023). These crack arrays preserve shock wave traces through previously solid material that we suggest to have been present within the center of the volcano through which the new 850 m deep crater developed during the eruption. Satellite and meteorological balloon data acquired for this eruption have also enabled quantification of the magnitude of water (~150 Tg), sulfur (0.4 Tg), HCl and HBr released into the atmosphere (Evan et al., 2023; Millan et al., 2022).

3. Discussion

The atmospheric and bathymetric data for the 2021–2022 Hunga eruption sequence together provide a basis for detailed analysis of the sequence of events that led to the climactic 15 January Hunga explosion. Firstly, however, it is necessary to review aspects of the structure and dynamics of active volcanoes. Most of these models constrain the behavior of magmas and 'volatiles' by invoking *plumbing* systems mapped as *conduits* and bound by impermeable and solid walls. Yet by observation, we know the rock masses that constitute a volcano are highly fractured and porous (Heap et al., 2018) and cannot operate as closed wall conduits. The upper part of a volcano may more realistically be modelled as a *gas-saturated, fractured porous medium* through which high temperature reactive gas expands from magmatic source to surface. In such media the overall flux is determined by a function of both the rock porosity and the high permeability of the fractures (Berre et al., 2019). Its dynamics are those of an open system gas reservoir constrained by its permeability and punctuated by dyke intrusions. As is also advocated by Girona et al. (2015), this suggests that understanding eruption dynamics may appropriately be approached through the chemistry and physics of the gas phase that has been released into the volcano from a magmatic system rather than restricted to in-magma gas-melt phenomena in isolation. This gas phase is usually referred to as a magmatic gas (or vapor) or a volcanic gas in large part depending on context.

3.1. Physics and chemistry of magmatic vapor plumes inside volcanoes

Water dominates the composition of volcanic gas mixtures (Fischer and Chiodini, 2015; Giggenbach, 1997) and is accompanied by CO_2, SO_2 and HCl plus a wide range of minor species, including metals. The median composition for gas mixtures recovered from high-temperature (i.e., 800 to 1000 °C) fumaroles on sub-aerial arc volcanoes is 90 mol % H_2O (Henley and Hughes, 2016), while CO_2 is the second most important component of volcanic gases at around 10 mol%. Gas phase solute content is typically <1 wt% (wt%) $NaCl_{equivalent}$ (Henley and Seward, 2018) so that first-order models of gas phase dynamics in volcanoes may adopt the thermochemical and thermophysical properties of pure water. On this basis, magmatic gas expansion through a volcano may be plotted in pressure-temperature space (Fig. 5) with a divergence point (X) from isentropic ($\Delta S = 0$) to isenthalpic ($\Delta H = 0$), where S is entropy and H is enthalpy. At X, higher permeability allows irreversible isenthalpic expansion to the surface. Kieffer and Sturtevant (1984) took a similar approach in considering the thermo- and fluid dynamics of the 1980 Mount St Helens eruption.

Magmatic gas released from intrusive centers below volcanoes must expand throughout the fractured porous rock mass of the volcano to form a coherent *magmatic vapor plume* (Henley and McNabb, 1978). Where the magmatic gas flux is high, the bounding interface between the gas and surrounding groundwater (seawater for submarine volcanoes) is defined by step differences in density, viscosity and wetting capacity between liquid and gas phases as well as by the availability of fracture intersections. For water-rich gas mixtures, condensation at the interface is limited by heat and mass transfer constraints. For low gas flux then scrubbing occurs into groundwater with little or no surface expression of the magmatic vapor release other than, in some cases,

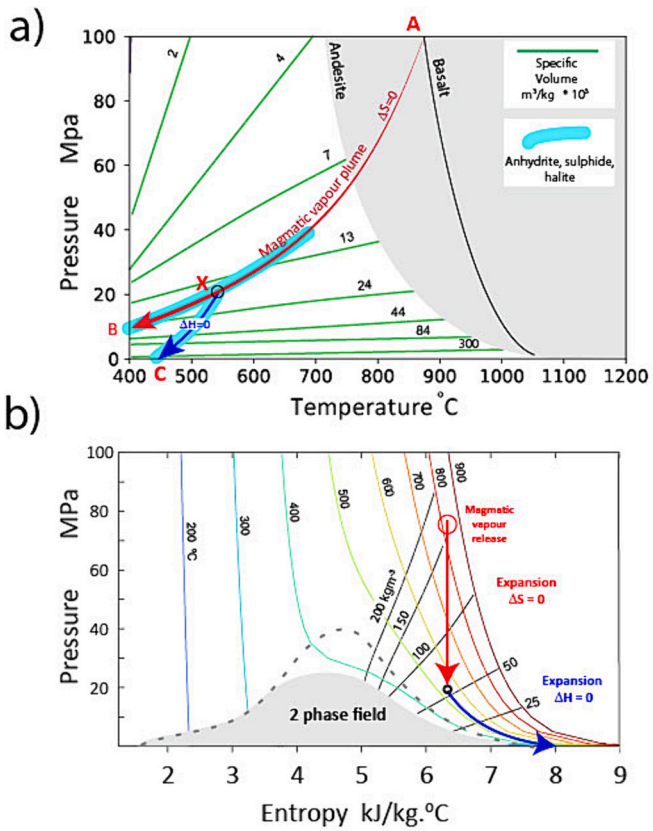

Fig. 5. Projection of isentropic and isenthalpic expansion curves for magmatic gas released below the Hunga volcano using pure H_2O as a proxy for volcanic gas. For details, see text and for further description of phase relationships in energy-pressure space see Mernagh et al., 2020, Driesner (2007); Driesner and Heinrich (2007). a) is a projection in pressure-temperature (PT) space in relation to minimum melt fields for reference magmatic compositions. It shows the steady isentropic expansion ($\Delta S = 0$) of released magmatic gas (Path A to B) with respect to its specific volume through to the surface through the rock mass above the intrusive source. At X a failure occurs, or the expanding gas enters a higher permeability regime and expands isenthalpically ($\Delta H = 0$) to the surface (Path X to C) with much larger relative volume increase. Also shown in the figure is the range of pressure and temperature over which the expanding gas phase deposits salt in a system containing ~1 wt% $NaCl_{equivalent}$ and over which gas-solid reactions deposit anhydrite and sulfides as cementing materials in feeder crack arrays with a consequent decrease in permeability. The P ordinate refers to the pressure of H_2O. b) Projection of isotherms and isochores of specific volume onto entropy-pressure space for pure water showing how magmatic gas expansion does not encounter two-phase conditions until very low pressures and so may be regarded as single-phase expansion. The dashed line schematically shows the expansion of the two-phase field of the NaCl-H_2O system with the addition of CO_2 and salts; the ordinate P then refers to the sum of P_{H2O} and P_{CO2} plus other minor gases.

weak discharge of insoluble gases such as helium.

Modern understanding of such magmatic vapor plumes is based on extensive studies of the exposed interiors of ancient arc volcanoes – some of which are now recognized as mineable *porphyry copper deposits* –(Henley and Berger, 2013; Henley et al., 2022; Mernagh et al., 2020). Plume dynamics are constrained by the rate of gas release from the magmatic system, the dynamical permeability structure of the volcano, and conservation of heat and mass through the system. In a steady state, sustained gas expansion through the fractured porous rock that constitutes a volcano is adiabatic (Henley and Hughes, 2016) and reversible. Gas expansion is irreversible near the surface where much more permeable fracture arrays are available, such as those beneath fumaroles. As an illustration, consider the release of 1 wt% water from an arc

magma at a pressure of 100 MPa (1 kbar, or ~ 3 km depth in the crust) and 1000 °C. Using steam table data (Wagner and Kretzschmar, 2008), the volume of the released gas increases five-fold during depressurisation to ~20 MPa assuming reversible adiabatic expansion through the mass of fractured porous volcanic rock. If permeability increases at shallower depths due to, for example, more abundant fracture permeability, expansion becomes irreversible and isenthalpic, with the specific volume of the gas phase >50 times higher at the surface than the initial exsolved volume (Fig. 5). For subaerial volcanoes, the occurrence of high temperature summit and flank gas discharges requires that the plume gas pressure exceeds the hydrodynamic pressure of surrounding crustal water that would otherwise flood the system. The balance of internal and external pressures allows magmatic vapor plumes to expand or contract in response to changing gas release rates from the underlying magmatic system as it evolves.

The near surface topology of a plume is affected by superimposed heat transfer processes. For example, interaction with perched groundwater regimes and downward flow of gas condensate in a subaerial volcano are shown in a plume schematic given in Henley and Hughes (2016). Downward flowing condensate is highly acidic and oxidized due to interaction with the atmosphere and results in intense solfataric alteration that may be associated with metal enrichment (Henley and Berger, 2011). Condensation and oxidation of discharged volcanic gases at surface also produce acidic volcanic lakes (Henley, 2015). Such a lake developed between the December 2021 and January 2022 eruptions (Fig. 2b) and evolved to a gas discharge plume prior to the main eruption. Subaerial solfatare may also have occurred around the cone built between the two islands at this stage (Figs. 2b and c). As noted in the Supplement to this paper, a lake was also present in association with cone formation during the 2014–15 eruption cycle.

Features such as volcanic lakes testify to the sustained flux of volcanic gases through the volcano superstructure. Similar evidence of sustained gas release also occurs beneath the seawater interface in submarine volcanoes, as determined from visual observations made by submersible and remotely operated vehicle surveys along the Tonga-Kermadec arc (de Ronde et al., 2007; de Ronde et al., 2005b; Lupton et al., 2008; Massoth et al., 2003). These gas release phenomena are also evidenced by sensor measurements of hydrothermal plumes in the water columns overlying submarine volcanoes (Sakuno, 2021; Sakuno et al., 2023) and the recognition of molten sulfur lakes at the summit of some submarine volcanoes (de Ronde et al., 2007; de Ronde et al., 2015). Shallow submarine gas discharges occurred from Hunga during the quiescent period immediately before the 15 January eruption (Figs. 2c and d) and several months *after* the eruption >50 bubble flares were observed, primarily within the crater, as acoustic water column reflectors in multibeam data (Ribo et al., 2023). An uncrewed surface vessel survey 6 months after the eruption deployed various sensors through the water column to a depth of 300 m that indicated that the bubbles were most-likely dominated by CO_2, providing evidence for ongoing volcanic activity (Walker et al., 2022).

SO_2 and HCl are significant components of volcanic gases (Fischer and Chiodini, 2015), causing the expanding magmatic gas mixtures inside volcanoes to be highly reactive. This sustains rapid solid-gas reactions involving calcium aluminosilicates, including plagioclase (Henley et al., 2015; Henley and Seward, 2018). These alteration and precipitation reactions have been shown to be a principal control on the total sulfur in discharged volcanic gases due to sub-surface sequestration of sulfur into anhydrite and sulfide (Henley and Fischer, 2021). The importance of these reactions is that they seal connected porosity, including microfracture arrays through which they expand (Henley et al., 2022), leading to reduction in gas flux and increase in gas pressure. Maintaining permeability then depends on refracturing over a range of scales due to tectonic stress and to release deviatoric stresses within the volcanic structure.

A schematic of a magmatic vapor plume sustained by gas release from deep seated intrusive activity and its expansion through the Hunga volcano is provided at true scale in Fig. 6. Also included schematically is a relatively high permeability central 'damage' core (or chimney) through the volcano that developed during long histories of repetitive eruption and infill by pyroclastic rocks as proposed for other volcanoes by Giggenbach (1990) and Reyes et al. (1993),. The high permeability of this régime vertically channels magmatic vapor flow as well, therefore, as focusing gas-solid alteration reactions that produce anhydrite ($CaSO_4$) and sulfide minerals. Choking of gas flux by these reaction products builds a sealing regime trapping compressed magmatic gas beneath it. Subsequent failure of this sealing regime is the primary component of the mechanism for the massive Hunga eruption of 15 January 2022 that we develop below. Seawater convection has been mapped on the flanks of other oceanic volcanoes and, through the inverse solubility of anhydrite, separately causes localized sealing on the outer carapace of a volcano (de Ronde et al., 2005a).

Taken together these chemical and physical components provide an alternative context for analysis of arc volcanoes as *large scale gas phase chemical reactors* (Henley and Berger, 2013; Henley and Seward, 2018).

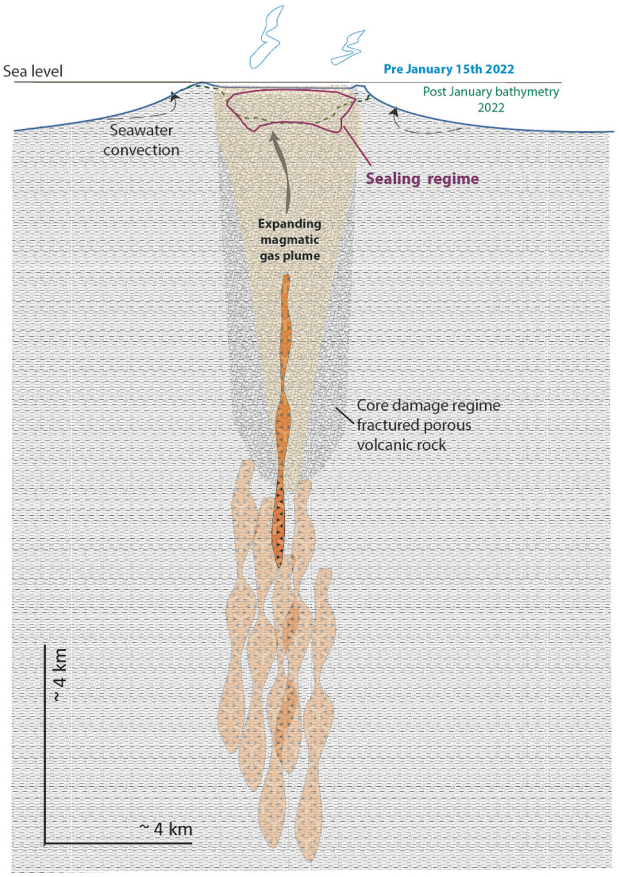

Fig. 6. Schematic pre-eruption view of a magmatic vapor plume (orange) expanding through fractured porous volcanic rocks to the seafloor in Hunga volcano, prior to eruption. The topography of the volcano is shown before (blue) and after (green) the eruption as discussed in the text and Fig. 3. Magmatic gas is sourced in a dynamical magma complex at a depth of a few km and expands to the surface through the volcano with enhanced flux provided by fracture arrays around the magma complex and through the core damage regime (circle symbol) of the volcano that developed from previous eruptions through the whole history of the volcano. The most recent dyking associated with gas release is shown as dark red in comparison with the lighter red representing a history of development of the sub-volcanic magma complex. Whilst the magmatism is dominantly as dykes in a trans-tensional arc environment, sills are also present as part of the general mass transfer of magma (Brenna et al., 2022; Cashman et al., 2017). For simplicity submarine flank seepages are not shown here. (For interpretation of the references to colour in this figure legend, the reader is referred to the web version of this article.)

They are continuously-evolving structures punctuated by penetrative heat and mass flow in the form of intrusive rocks. Their growth and form generate inherent deviatoric stress instabilities in terms of potential slope failure (Bak, 2013) and aggressive gas-solid reactions that control internal gas pressure and flux. It is this dynamical systems approach that enables analysis of the energetics and time sequence of the Hunga eruption in contrast to reductionist approaches focused on single phenomena.

3.2. Eruption mechanism and sequence of the 2022 Hunga climactic eruption

Seismic data suggests that an initial earthquake and the main explosive phase of the Hunga eruption occurred within a few seconds of each other (Thompson et al., 2022). This observation is important when considering the explosion mechanism itself. Here, we propose that the climactic Hunga eruption was triggered by hydraulic failure of the subsurface rock mass and that this failure event was recorded through the seismic signals emitted from 04:00 to 04:16 UTC. There was precursor activity, including infrasound wave propagation and large explosive events, in the month prior to the climactic event (Matoza et al., 2022). These events indicate that the volcano was perched at a *critical* stability state (Bak, 2013) punctuated by small releases of energy and mass as steam and ash. The subsequent massive explosion and gas release at 04:15 UTC indicates that the energy state of the volcano had continued to increase through this precursor period until hydraulic failure of the sealing regime occurred. This may have occurred at a number of sites across the volcano and rapidly coalesced as material was eroded into the discharging gas. At this time the energy state of the volcano had become *supercritical* as defined by the escalation of the masses of eruptive products including gas and particulates into the fast-growing major ash plume. Mass removal excavates the crater whose deepening provides positive feedback through releasing higher- and higher-pressure gas from the porous rock mass. The eruption declines and ceases when this reservoir of compressed gas becomes depleted and seawater can then back fill the crater. The occurrence of gas bubble flares months after the eruption provides evidence for the continued depletion of this gas reservoir.

3.3. Hydraulic failure inside volcanoes

For a rock mass that contains compressed gas, tensile failure occurs where the pore fluid pressure exceeds the sum of the least principal confining stress plus the pore pressure in the rock mass and the tensile strength of the rock (Cox, 2010; Engelder et al., 1990; Phillips, 1972; Secor, 1965). Tensile failure data for volcanic rocks (Heap et al., 2022) provide a useful tensile strength reference value of ~2.5 MPa for porosities of 10 to 30%. Such failure is marked in mineral deposits by distinctive vein textures as well as breccia bodies. Notably, porphyry copper deposits that formed in ancient volcanoes are typified by the presence of breccia bodies and pebble dykes, as well as by the extensive stockworks of fractures that supported gas flux through them and consequent mineralisation. These features record a continuous cycle of tensile failure and sealing by anhydrite, sulfide, quartz and other silicate minerals (Henley et al., 2022; Mernagh et al., 2020) that occurs in active degassing volcanoes today as is evident from micro-seismicity (McNutt, 2005). We note that these minerals have been reported in erupted lithic fragments of Hunga volcano (Hamilton, 2023).

For a system through which reactive volcanic gas fluxes to the surface, the sealing (or choking) of connected porosity by gas-solid reactions (Henley and Fischer, 2021; Henley et al., 2022; Henley and Seward, 2018) leads to increased gas pressure beneath the seal because the deeper magmatic system continues to release gas at lithostatic pressure into the volcano. If the increase in gas pressure below the seal exceeds the effective tensile strength of the sealed rock mass, then failure is imminent. In volcanic systems, the initial stresses tend to be tensile (also called open-mode fractures as these 'open' the system, and precede shear stresses) which are responsible for rock/magma fragmentation processes (Heap and Violay, 2021).

Tensile failure provides a highly transmissive path for pressurized gas to escape through the fractured seal into the lower pressure regime at shallower crustal levels in the volcano superstructure, or directly to the ocean and atmosphere. Such rapid expansion may be explosive and, consequently, able to remove rock mass at, and above, the seal and further reduce the confining stress. Loss of gas also reduces the gas pressure near the failed seal so that the gas pressure from the deeper reservoir to that point increases. It is these responses that, through positive feedback, build the stress state toward a major explosive event. Thus, once initiated as a small event, the magnitude of the eruption continually increases as lithostatic load is removed until the compressed gas reservoir becomes depleted and the eruption declines (Henley and Hughes, 2016). The eruption energy may be further amplified by decompression of gas-saturated rock mass that does not contain *connected* porosity (Scheu and Dingwell, 2022).

In this context, Fig. 7 provides a schema for pore gas pressure through Hunga volcano prior to the 15 January eruption. Magmatic gas is released from an active subsurface magmatic complex, shown here at about 2 km below sea level, that sustains a gas flux to the surface through a magmatic vapor plume. Note that the internal gas pressure of this plume (path aa) is greater than the external pressure of seawater. The pressure distribution consequent on sealing or choking by alteration reactions at some depth is shown as path bb in Fig. 7. At this point the gas pressure gradient has decreased so that quasi-magma source pressure is transmitted from below to the sealed region. This can only be sustained until the differential between gas pressure and lithostatic pressure at the seal exceeds the tensile strength of the sealed rock mass. Increasing gas pressure leads to hydraulic failure, with the compressed gas phase rapidly expanding toward the surface, removing existing mass in its path as pyroclastic material. We suggest that this pressure cycle was initiated, prior to the 19 December 2021 ash plume-forming eruptions, by an increase of magmatic activity over several weeks or months prior to which the volcano had been essentially inactive or weakly passively degassing. Between 04:00 and 04:15 UTC on 15 January, isolated hydraulic failures and explosive gas release ("gunshot sounds") commenced within the sealed rock mass which had developed in the upper part of the volcano. The consequent discharge grew rapidly to develop an ash plume by 04:10 UTC with removal of near-surface mass. The consequent decrease in load pressure extended downward through the gas-saturated reservoir of rock within the now developing crater. Further hydraulic failure was sustained until the fracture array reached a percolation threshold (Cox et al., 2001) that enabled very rapid release of the potential energy stored as a reservoir of compressed gas through the mass of the volcano. Coalescence of gas discharge in this way encompassed a large volume of compressed gas that expelled upward, displacing overlying seawater. We suggest that this was manifest as an extensive 'bubble' at the surface whose collapse developed a major tsunami (Heidarzadeh et al., 2022; Lynett et al., 2022; NOAA, 2022; Pakoksung et al., 2022; Purkis et al., 2023). We further suggest that the gas 'bubble', including the column of gas in the developing crater below it, then exploded into the atmosphere, generating a near-surface blast that released the spectrum of acoustic-gravity waves that accompanied the eruption between 04:15 and 04:37 UTC. This sequence of 'balloon' expansion and collapse at the sea surface has been recorded for underwater nuclear explosions and is discussed by Best (1991).

Positive feedback on the eruption occurred from 04:15 UTC as rock mass was progressively removed, progressively excavating the 850 m-deep crater observed in the post-eruption bathymetric survey. In this supercritical phase rock and gas removal led to runaway changes in pressure gradients thereby building the power of the eruption. It is during this excavation period that limited volumes of silicic melt, present as dykes, may have been encountered which then decompressed to form pumice that, as a relatively minor component of the pyroclastic

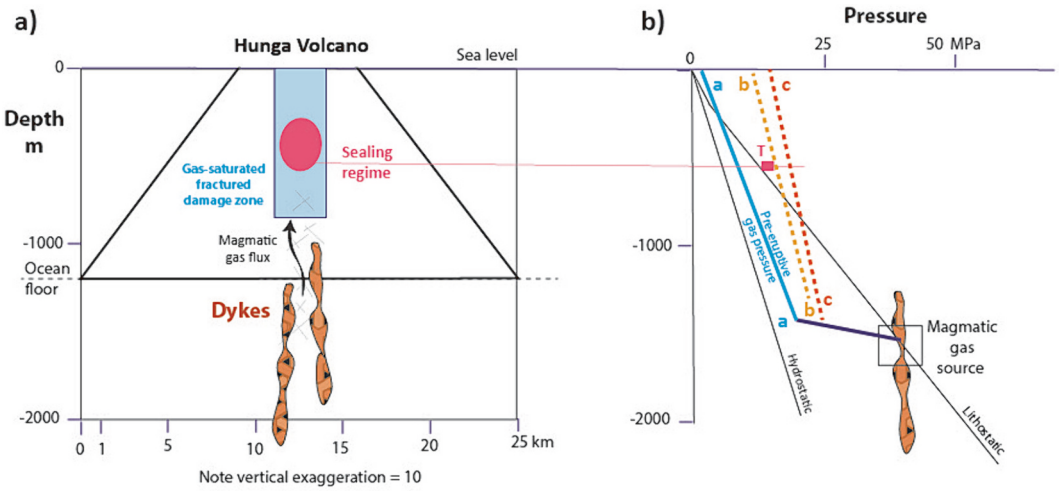

Fig. 7. Compressed gas-tensile failure or core blow-out model for the Tonga eruption. a) summarises the spatial relations between sub-volcanic intrusions that release magmatic gas which then expands through the high permeability damage zone in the core of the volcano to sustain a magmatic vapor plume as described in the text. Gas-solid reactions progressively result in sealing of connected porosity to form a 'Sealing regime'. b) shows pressure-depth relations for an expanding gas relative to lithostatic and hydrostatic (seawater) pressure. Path aa is the unrestricted expansion path of the magmatic gas phase through the plume to discharge at the surface. Path bb shows the evolved path following sealing or choking of the gas expansion, leading to high pressure at and beneath the sealing regime. The tensile strength of the altered and sealed rock (T) then defines a critical stress state above which hydraulic fracturing occurs when total gas pressure exceeds the sum of the lithostatic and equivalent tensile strength. Path cc shows the gas pressure at failure when the system has become supercritical, and fracturing starts to explosively release compressed gas. This stage feeds upon itself through increased pressure gradients around the point of failure but eventually the eruption wanes as the large-scale gradient tends to the original state (aa) as the gas reservoir becomes depleted. The figure is necessarily schematic.

yield, was observed subsequently as pumice rafts. The cessation of the eruption commenced when the gas pressure within the volcano became depleted and the residual gas pressure could be accommodated by existing porosity, as is the normal case for exploitation of a petroleum gas reservoir. This terminal phase was marked by the progressive collapse of the atmospheric plume over a period of several hours following the main phase of the eruption.

3.4. *Gas-driven explosive eruptions*

Explosive gas release in igneous and magmatic systems has previously been suggested for Plinean eruptions such as Mt. St Helens in 1980 (Burnham, 1985). Burnham's second boiling mechanism was based on a *closed system* model centered on crystallization and vesiculation of a specific mass of water-saturated magma to develop an impervious solid carapace that failed hydraulically as internal gas pressure increased. Hedenquist and Henley (1985) independently developed an *open system* model for hydrothermal eruptions such as at Waiotapu, New Zealand where mineral deposition in the fractures that fed hot springs trapped CO_2-rich vapor that was released from the underlying geothermal system. Hydraulic failure of these seals resulted in hydrothermal explosions. A similar sealing model ($<10^{-3}$ km^3 pyroclastic) for minor phreatic eruptions such as Galeras (Colombia) in 1993 was proposed by Fischer et al. (1994) and by Christenson et al. (2010) for the 2007 eruption of Ruapehu's (New Zealand) Crater Lake. Thiery et al. (2010) and Girona et al. (2015) have since applied these approaches to the modelling of phreatic and magmatic hydrothermal eruptions and introduced the useful term '*gas-driven eruptions*' into the literature (Caudron et al., 2019). We formally adopt this term now for the much larger Hunga climactic eruption. However, we stress that the model developed here is at *whole-of-volcano scale* and does not involve direct heat transfer between magma and a fluid phase.

We propose that the major atmospheric disturbances generated by the 15 January 2022 Hunga eruption were due to the explosive release of compressed gas which had been trapped within the body of the volcano into the atmosphere, producing a massive air blast. We now consider how such a large mass of gas might be released over a short time, and what its pressure and temperature were before the commencement of the climactic explosive sequence. Our first order approach is based simply on the well-known Gas Laws and the First Law of Thermodynamics. It assumes that the initiation of the eruption was by hydraulic fracture of a choked or sealed gas reservoir within the volcano, and that the consequent isenthalpic expansion of compressed volcanic gas from high to low pressure occurred explosively.

The principal driving component of any volcanic explosion is the pressure-volume-temperature (PVT) expansion energy of the compressed gas in the reservoir of connected pore space (the magmatic vapor plume) within the whole volcanic structure. When released, some of this potential energy partitions into fragmentation and kinetic energy components which constitute the pyroclastic yield of the eruption. The remainder may be classed as *excess energy* which, for Hunga, was expressed primarily as acoustic-gravity waves, including Lamb waves (Matoza et al., 2022), as the compressed gas exploded and displaced the atmosphere at sea level. Some excess energy will, in general, support thermal forcing of the atmospheric eruption column, but this portion is not dominant in this case. A small proportion was also expressed as tsunamic waves centered on the volcano.

The energetics of the 15 January eruption may therefore be simply constrained using the First Law of Thermodynamics. First, we define a *control volume* as the region within which sudden and irreversible compressed gas expansion and rock displacement occurs (Fig. 7). We suggest that the excavated crater defined by the 2022 bathymetric survey defines this control volume for the 2022 eruption sequence. During the eruption sequence we consider that the mass flux of magmatic gas into the control volume was negligible, so that the mass of compressed gas sealed within it then defines the maximum amount of potential energy release (ΔE), including thermal energy, that controls the eruption, since,

$$\Delta E = E_i - E_f = m_g h_g + m_r c_{p,r} \Delta T_r \quad (1)$$

where subscripts i and f refer to initial and final states, m_g and m_r are the masses of compressed gas (subscript g) in the porous rock (subscript r), h_g is the specific enthalpy of the gas, $c_{p,r}$ is the specific heat capacity of the rock and ΔT_r is the temperature difference between the gas-saturated porous rock and the atmosphere.

We first make an estimate of the required energetics if only the release of compressed gas was involved. Neglecting the second term on the right-hand side of Eq. (1) and assuming that ΔE was of the order 1EJ, then the mass of compressed gas must be at least.

$$m_g \approx \frac{\Delta E}{h_g} \approx 10^{18} \Big/ 3500 \times 10^3 \approx 3 \times 10^{11} kg \quad (2)$$

This estimate assumes the specific enthalpy of the compressed gas is approximately 3500 kJ/kg at the assumed initial conditions of $T = 600$ °C, $P_g \sim 21$ MPa, and that the vast majority of this enthalpy is converted into work energy as the gas is released to atmospheric pressures (e.g., via an explosive isenthalpic expansion into the atmosphere (Anderson and Crerar, 1993)). For the above initial conditions, the specific volume of the compressed gas is $v_g \sim 0.015$ m^{3}kg^{-1}; therefore, the compressed gas volume prior to the explosion would be about 4.5 km^3. For this *gas-only* model, this volume is unreasonable given that the control volume was about 6.5 km^3.

The preceding estimate prompts calculation of the role of thermal energy from the rock mass in the explosive eruption. Prior to the eruption, we assume that the rock is heated to the local temperature of the trapped compressed gas by hydrothermal circulation through the porous matrix. Given the range of depths that the erupted rock volume occupies initially, we estimate a representative bulk temperature for the rock to be 600 °C. Thus, if the volume of rock that is to be removed by the eruption is V_r, we estimate the overall release of thermal energy during the eruption by writing Eq. (1) in the form,

$$\Delta E \approx \frac{V_r \Phi}{v_g} h_g + V_r (1 - \Phi) \rho_r c_{pr} \Delta T \quad (3)$$

where ρ_r is the density of the rock, ϕ is the connected porosity and the temperature decrease of the rock ΔT ($\leq \Delta T_r$). Taking $\phi = 10\%_{\text{volume}}$, the first term of this equation equals about 0.15EJ. The second term provides the potential thermal energy transfer from the rock as it cools toward the local ambient temperature, which will tend to depend on both location and time. For example, if the immediate expansion of the compressed gas is isenthalpic, we would expect its temperature to decrease rapidly in the first instance to approximately 500 °C at atmospheric pressure. With a temperature difference of approximately $\Delta T = 100$ °C between the rock and surrounding gas, $c_{pr} = 840$ J K^{-1} kg^{-1} and $\rho_r = 3000$ kg m^{-3}, the thermal energy associated with the second term (i.e., that would be released locally from the erupted rock) is about 1.5 EJ, which is consistent with the energy that would be required to provide about 1 EJ for the atmospheric disturbance and waves. This approach demonstrates the importance of rapid heat transfer from the rock to the decompressed gas phase, which is sustained by rock fragmentation to provide a relatively large surface area of hot rock. Heat transfer also occurs during mass transfer and expansion of the particulate rock-gas mixture in the jet phase of Plinean volcanic eruptions (referred to as a pseudo-gas by Kieffer and Sturtevant (1984)). Moreover, there is a remaining temperature differential between the erupted rock and the surrounding atmosphere (which we estimate to be an average of almost 500 °C if the atmosphere is about 20 °C); thus the potential remains to release up to a further 7.5 EJ in thermal energy by heat transfer from the fine-grained erupted volcanic rock into the gas phase in the developing volcanic ash plume.

The magnitude of the *total* explosion energy released to the atmosphere in the 15 January Hunga eruption has been estimated as between about 0.1 and > 20 EJ. This range may be accommodated in this schema by adjustment, primarily, of the assumed porous rock control volume and its effective porosity; here we have initially constrained the control volume to that of the final state crater. Taking the 20.8 EJ high-end estimate of Matoza et al. (2022) would imply that the control volume was larger and/or that the effective porosity was proportionately larger.

The early stages of the eruption comprised several explosive events, some of which were recorded as 'gunshot' sounds. This phenomenon is consistent with bursts of gas at different locations across the 11.5 km^2 surface area of the developing vent. Such compartmentalization of the explosive sequence by interplay of subsurface gas pockets (Girona et al., 2019), is suggested by the scallop-shaped, semi-circular features on the inner southern wall of the crater (see Fig. 3b). These coalesced to form either the major "bubble" mound, similar to the gaussian initial conditions of Heidarzadeh et al., 2022 and NOAA, 2022; or breakthrough cavity with rim waves (Lynett et al., 2022; Pakoksung et al., 2022; Purkis et al., 2023) for tsunami generation. All the tsunami models reference here estimate at least 100 m-high waves and/or 100 m-deep water cavity are needed to explain the tsunami amplitudes and flooding on nearby Tonga islands, which is consistent with the observations presented here, but may need to be revised upward in future assessments. It was the breakthrough of the fast-expanding gas through the water layer that generated the tsunami wave locally and the atmospheric blast heard around the world. Alvarez and Camacho (2023), based on satellite gravity data, have suggested that sub-surface Hunga contains several lower-density rock compartments. The scale of the evolving crater-forming (or emptying) eruption suggests to us that multiple hydraulic failures were generated as pressure waves rapidly spread. Zheng et al. (2023) identified 3 separate seismic events with similar force-equivalent evolution history in the 300 s period immediately after the main explosion and suggested that these may be ascribed to a model of 'magma hammer'. This model however assumes a closed conduit volcano model and the direct involvement of magma in the overall explosive event but, we suggest, is precluded by the spatial scale of the eruption and its continuation beyond this short time. It is, however, possible to consider that these signals were due to a similar compartmentalization of the decompression of gas—or by that stage a higher density pseudo-gas containing particles (Kieffer, 1984)—in the upper part of the developing vent. Such compartmentalization is a likely consequence of the relative rates of shock wave propagation through the heterogenous porous gas-saturated rock mass with resonating sequences of compression-decompression resulting in fine scale fragmentation, in similar fashion to efficient blasting techniques in modern mining. It is useful to note here that the popular, but closed system, 'pressure cooker' model for volcanic eruptions is simply an analogy - unless of course the safety valve is welded shut! More illustrative of the explosive power of gas explosions are the catastrophic and deadly boiler explosions on steam powered Mississippi riverboats (Lloyd, 1856) as well as destructive steam engines explosions (https://www.vintag.es/2020/02/steam-locomotive-boiler-explosion.html) in the early decades of steam locomotion.

Other evidence for the explosion model that is developed here includes the quiescent period observed by satellite immediately prior to the eruption. We interpret this period as indicating the completion of the sealing process in the core of the volcano so that surface discharges ceased. Underwater seepages continued due to the increased pressure below the sealed region (Fig. 2c).

The mass of water-dominated gas calculated by our first order model is 5.3 × 10^{10} kg which compares well with the 1.4 to 1.5 × 10^{11} kg estimate of total water released into the atmosphere (Evan et al., 2023; Millan et al., 2022; Xu et al., 2022). However, as noted by these and other authors, there is an apparent deficit in total sulfur emission of the Hunga eruption relative to other volcanic eruptions, such as Pinatubo in 1991 (Carn et al., 2022; Millan et al., 2022; Xu et al., 2022) and that this deficit appears to be characteristic of underwater eruptions. It has been suggested (Legras et al., 2022) that the apparent deficit in SO_2 emission was a consequence of rapid, in-plume conversion to sulfate aerosol. These authors estimated an emission of 187 kt of SO_2 during the eruption. Using a median value for the SO_2 content of arc volcanic gases of 1.25 mol% (Henley and Hughes, 2016) and our estimate of the mass of volcanic gas involved in the initial explosion, we estimate ~220 kt SO_2 would have been emitted. The difference between these two values is consistent with the suggestion of loss of SO_2 by reaction with feldspars in the volcanic rock mass (Henley and Fischer, 2021; Henley et al., 2015;

Henley and Seward, 2018; Renggli et al., 2019) to form anhydrite during the choking or sealing of the volcano prior to the 15 January eruption. Experimental studies have shown that these gas-solid reactions are fast, such that sealing occurs rapidly within a high temperature fractured porous rock mass, as may be inferred for the smaller 2016 phreatic eruption of White Island (Christenson et al., 2017). Estimates of the rate of SO_2 scavenging by rhyolite-gas reaction have been provided by Casas et al. (2019). For Hunga in this context, it is noteworthy that a petrographic study of post-eruption non-juvenile lithic pyroclastics (Hamilton (2023) reported that hydrothermal alteration was common, and that the observed secondary minerals include anhydrite/gypsum, pyrite, chalcopyrite and quartz. Such alteration is consistent with the occurrence of gas-solid reactions attending SO_2 streaming through the volcano's core prior to eruption. These observations, and the apparent sulfur-deficit in the volcanic plume, are also consistent with the observed discharge of discolored water from the inner and outer flank of the tombolo immediately prior to the eruption (Fig. 2d). Such discharges have been observed elsewhere on submarine volcanoes and shown to be due to the generation of alunite and native sulfur as well as sometimes being associated with pyrite chimneys (de Ronde et al., 2005a; de Ronde et al., 2011). Anhydrite deposition from heated seawater circulating within the outer carapace of the volcano may have contributed to the overall sealing process prior to the eruption.

We suggest that the eruption model outlined above quantitatively accounts for the Hunga eruptive sequence and energy release, but it is appropriate to briefly consider other models that have been proposed. As an intra-oceanic volcano, the Hunga eruption was quickly ascribed in media reports to a fuel-coolant, phreatomagmatic type explosion involving direct interaction of seawater with lava at around 1000 °C. The limiting parameters for such explosions are the surface area over which the heat transfer occurs, the mass of coolant and the heat of evaporation of the coolant. For water, the latent heat of vaporization at high temperatures (or a low salinity seawater liquid phase) is 3000 to 3500 kJ/kg (Wagner and Kretzschmar, 2007). On this basis, the explosive energy of a 4.2 EJ eruption would require the maximum possible instantaneous heat transfer from at least 1.7 km^3 of magma to 1.2 km^3 of seawater. For sufficiently rapid heat transfer, the length scale of prior fracturing of the magma, as a lava, is of the order of one centimeter over the entire volume of the interaction and implies unreasonably high connected porosity. Again, satellite data provide no evidence of the generation of a large near surface lava lake prior to the eruption.

Another model that has been suggested in discussions of the Hunga eruption is caldera collapse (e.g., Kulichkov et al., 2022). There is, however, no specific evidence for this to have occurred and Alvarez and Camacho (2023) have specifically suggested that 500 m resolution gravity data do not indicate the presence of a magma chamber to 6 km below the volcano. Moreover, the coincidence of the morphology of the post-2022 eruption crater with pre- eruption morphology suggests there has been no significant collapse. Tilted roof blocks of rock, or step faults that would be indicative of roof collapse are also not evident in the bathymetry. Similarly, the bathymetry does not indicate any major flank collapse features outside the crater rim, nor are there any newly formed volcanic cones outside the volcano flanks. A large breach in the northeast rim of Hunga (Fig. 3) may be the result of the blast from the intense gas-driven explosion or due to scouring and erosion consequent to the large density currents that occurred during collapse of the volcanic plume.

3.5. The Hunga eruption in a wider context

The Hunga eruption had a pyroclastic yield equivalent to that of several other major Plinean eruptions throughout Earth history. The singularity of this eruption was the wide range of quantitative energetics data that was obtained for the cataclysmic phase of the eruption. Our ability to monitor the generation of acoustic-gravity waves worldwide that have enabled estimates to be made of the magnitude of its explosive energy. For example, the scale of wave propagation from Hunga matched and likely exceeded that of the 1883 Krakatau eruption. Our analysis suggests that the Hunga eruption was a consequence of hydraulic failure and explosive pore gas release to locally generate an extreme runup tsunami, and a near surface air blast that generated the acoustic-gravity wave response in the atmosphere which then contributed to tsunami generation in the Pacific and globally. The increase in gas pressure within the volcano and its explosive release was a consequence of magma-derived gas flux through the volcano and the sealing capacity of minerals formed by gas reactivity with the volcanic host rocks. As such, the Hunga eruption sequence was independent of its oceanic setting and its promulgation was like that of sub-aerial Plinean eruptions. An implication of the model is that large submarine eruptions can occur at any seawater depth because the driving pressure is transmitted from the deep magma source regime and not from the higher-level intrusions derived from it. For a deep sea eruption, the gas blast itself, however, may dissipate before reaching the surface, as appears to have been the case for the 2012 Havre eruption (Manga et al., 2018) that was manifest only by widespread pumice rafts at surface. The detailed analysis of the 1650 tsunamigenic Kolumbo (Greece) eruption (Karstens et al., 2023) also provides a record of cascading energetics that we suggest may be similar to the gas-driven model discussed in this paper. In this case flank failure may have been the immediate trigger that released the internal gas pressure that had developed within the volcano.

A key feature of the Hunga eruptive sequence was the cessation of significant surface activity for a short period immediately before the Plinean explosion. Similar eruptive behaviours have been traced through many eruptions that have impacted the course of human history (Oppenheimer, 2011). It is well documented for the 1991 eruption of Pinatubo, with a sequence of steam eruptions prior to a major precursor eruption and a quiescent pause immediately before the VEI 6 eruption that dispersed over 10 km^3 of pyroclastic material (Fischer et al., 1994; Newhall and Punongbayan, 1996). The acoustic-gravity wave propagation of this eruption was, however, an order-of-magnitude less than that of Hunga. The Mount St Helens Plinean eruption in 1980 was also preceded by a sequence of steam-blast activity and seismicity (Christiansen et al., 1981) and the Tambora eruption of 1815 similarly commenced through a series of minor to major episodes including "cannon fire" prior to its VEI7 cataclysmic eruption. This eruption was reported to have been audible almost 5000 km away. More recently, periods of diminished fumarolic activity were recorded by Yamaoka et al. (2016) prior to the several eruptions of Mt. Ontake (Japan) in 2014. Indeed, periods of quiescence associated with long period seismicity appear to be a characteristic of what, here, we interpret as gas-driven eruptions from small to climactic scale.

We therefore suggest that the common source of major explosive energy for Plinean eruptions is the energy stored in compressed, magma-derived gas within the bulk of a volcano, and that climactic eruptions are triggered by hydraulic failure of alteration-sealed volcanic rocks. Magmatism is not considered to be the immediate, *direct* cause as is generally assumed for both for these, and for lower magnitude, phreatic and phreatomagmatic eruptions.

4. Summary and conclusions

The scale of the explosive energy released ($>>4$ EJ) by the 15 January 2022 climactic eruption of Hunga volcano has been estimated from the amount of ejected material (>6.3 km^3), mass eruption flux ($\sim 5 \times 10^9$ kg s^{-1}), height of eruption column (58 km), atmospheric gravity waves, earthquakes, and meteotsunami. In turn this indicates that it was similar in scale or larger than the 1883 eruption of Krakatoa, Indonesia. Understanding the cause of such an eruption is crucial to building sensible monitoring programs for risk mitigation both in the vicinity of Hunga and other volcanoes around the world. Previous models have assumed magma-seawater interaction, but heat transfer

considerations show this to be untenable and direct evidence is not provided by satellite data. Suggestions of caldera collapse are similarly unsupported by bathymetry or by the seismic record of the eruption. Rather, the direct evidence for the cause of the cataclysmic explosive eruption lies within its time sequence through the eruption cycle commencing several weeks earlier and the observed energy release into the atmosphere.

In this paper we have taken a systems approach to develop an alternative model based on these data and fundamentals of gas phase heat and mass transfer in volcanoes. Explosive eruptions at this scale require the very rapid release of some store of potential energy which here we argue is the compressed magmatic gas sealed into the core of the volcano remote from its magmatic source. It is now well established that fast reactions occur between the SO_2 and HCl contents of magmatic gases to produce minerals including anhydrite, quartz and sulfides as they expand from source to surface through the fractured porous rock mass of a volcano. Their formation leads to choking of flow paths and potentially sealing of the gas flux through the volcano. In turn this results in rapidly increasing gas pressure beneath the sealed region to a critical point where hydraulic failure of the seal is inevitable. It is such hydraulic failures that enable irreversible gas expansion to occur as was seen as the explosive gas blast into the atmosphere on 15 January 2022.

At Hunga the hydraulic failure triggering step was also accompanied by release of seismic energy release and tsunami wave phenomena. The trigger also initiated the major ash plume that grew to a height of 58 km as it continued to mine gas and rock as the new 2-3 km diameter crater was excavated to a depth of 850 m. This stage of explosive activity feeds upon itself through rock removal and increased gas pressure gradients within the volcano. This supercritical state continued through the excavation of the new crater which at Hunga extended to 850 mbsl until the internal reservoir of compressed magmatic gas became too depleted (see Graphical Abstract) and the volcano returned to a quiescent state.

These same sealing minerals (e.g. anhydrite, sulphide) have been identified in the extinct volcano-hosted, intensively explored and mined occurrences of base and precious metal deposits (porphyry copper deposits) that have formed in arc-type volcanoes for over 400 million years. They have also been recorded in the ejecta of many explosive eruptions of Pacific Ring of Fire-type volcanoes, including Hunga.

We here suggest that such a mechanism of gas-driven eruption is characteristic of Plinean-type eruptions whether in oceanic or subaerial volcanoes. Development of the conditions that may lead to Plinean scale catastrophic energy cascades, consequent on the failure of such mineral seals, is hard to predict. The occurrence of a quiescent pause in gas discharge or seismicity during an eruption cycle, as at Hunga, Pinatubo and Vesuvius, may be a warning of the possibility of an imminent gas-driven eruption, but we emphasize here that hazard monitoring for all volcanoes requires a consistent, long term, *whole-of-volcano* approach underpinned by gas monitoring, seismic and acoustic data.

Author agreement statement

We the undersigned declare that this manuscript is original, has not been published before and is not currently being considered for publication elsewhere. We confirm that the manuscript has been read and approved by all named authors and that there are no other persons who satisfied the criteria for authorship but are not listed. We further confirm that the order of authors listed in the manuscript has been approved by all of us. We understand that the Corresponding Author is the sole contact for the Editorial process. He/she is responsible for communicating with the other authors about progress, submissions of revisions and final approval of proofs.

Signed by corresponding author on behalf of all co-authors:
R.W. Henley.

Credit authorship contribution statement

Richard W. Henley: Writing – review & editing, Writing – original draft, Visualization, Methodology, Investigation, Formal analysis, Data curation, Conceptualization. **Cornel E.J. de Ronde:** Writing – review & editing, Writing – original draft, Investigation, Data curation, Conceptualization. **Richard J. Arculus:** Writing – review & editing, Writing – original draft, Investigation, Conceptualization. **Graham Hughes:** Writing – review & editing, Writing – original draft, Investigation, Formal analysis. **Thanh-Son Pham:** Writing – review & editing, Writing – original draft, Methodology, Investigation, Formal analysis, Data curation. **Ana S. Casas:** Writing – review & editing, Writing – original draft, Formal analysis. **Vasily Titov:** Investigation, Writing – review & editing. **Sharon L. Walker:** Writing – review & editing, Writing – original draft, Visualization, Investigation, Formal analysis, Data curation, Conceptualization.

Declaration of competing interest

The authors declare the following financial interests/personal relationships which may be considered as potential competing interests.

Cornell de Ronde reports financial support was provided by New Zealand Strategic Science Investment Fund. If there are other authors, they declare that they have no known competing financial interests or personal relationships that could have appeared to influence the work reported in this paper.

Data availability

Data will be made available on request.

Acknowledgments

As researchers we acknowledge that climactic eruptions cause major loss of homes and lives so that we hope continued exploration of their causes may help to mitigate future risk in many parts of the world. Richard Henley wishes to thank the Australian Academy of Sciences for encouragement and the provision of an opportunity to present this interpretation of the 2022 Tonga eruption: https://www.science.org.au/news-and-events/events/haddon-forrester-king-lecture-by-professor-richard-henley. We especially thank Steve Ingebritsen and Tobias Fischer for constructive review comments. We also thank Steven F. Cox and Fred J. Prata for useful discussions during the initial development of this paper. Thomas Donda is thanked for assistance with graphics. Cornell de Ronde acknowledges support from the New Zealand Strategic Science Investment Fund (SSIF). Thanh-Son Pham and Ana Casas Ramos, respectively, acknowledge financial support from the Australian Research Council through a Discovery Early Career Researcher Award (DE230100025) and Discovery Project Grant (DP200100406). This paper has been assigned a PMEL contribution number of 5570.

Appendix A. Supplementary data

Bathymetric analysis of the morphological changes of Hunga volcano prior to, and after, the 2022 eruption sequence. Supplementary data to this article can be found online at [https://doi.org/10.1016/j.jvolgeores.2024.108077].

References

Alvarez, R., Camacho, M., 2023. Plumbing System of Hunga Tonga Hunga Ha'apai Volcano. J. Earth Sci. 34 (3), 706–716.
Anderson, G.M., Crerar, D.A., 1993. Thermodynamics in Geochemistry: The Equilibrium Model. Oxford University Press.
Astafyeva, E., Maletckii, B., Mikesell, T.D., Munaibari, E., Ravanelli, M., Coïsson, P., Manta, F., Rolland, L., 2022. The 15 January 2022 Hunga Tonga eruption history as

inferred from ionospheric observations. Geophys. Res. Lett. 49 (10) e2022GL098827.
Bak, P., 2013. How Nature Works: The Science of Self-Organized Criticality. Springer Science & Business Media.
Baxter, R., White, J., Marino-Paredes, J., Cronin, C., Carey, R., Cassidy, M., Parh, S.-H., 2023. Particle morphologies and damage fractures created by high-energy eruptions: Comparing particles from Tonga's 2022 Hunga eruption with Krakatoa 1883, and Havre 2012 eruptions. In: Frontin-Rollet, G., Nodder, S. (Eds.), Geoscience Society of New Zealand Annual Conference 2023.
Beier, C., Turner, S.P., Haase, K.M., Pearce, J.A., Münker, C., Regelous, M., 2017. Trace element and isotope geochemistry of the northern and central Tongan islands with an emphasis on the genesis of high Nb/Ta signatures at the northern volcanoes of Tafahi and Niuatoputapu. J. Petrol. 58 (6), 1073–1106.
Berre, I., Doster, F., Keilegavlen, E., 2019. Flow in fractured porous media: a review of conceptual models and discretization approaches. Transp. Porous Media 130 (1), 215–236.
Best, J.P., 1991. The Dynamics of Underwater Explosions.
Bevis, M., Taylor, F.W., Schutz, B., Recy, J., Isacks, B., Helu, S., Singh, R., Kendrick, E., Stowell, J., Taylor, B., 1995. Geodetic observations of very rapid convergence and back-arc extension at the Tonga arc. Nature 374 (6519), 249–251.
Borrero, J.C., Cronin, S.J., Latu'ila, F.H., Tukuafu, P., Heni, N., Tupou, A.M., Kula, T., Fa'anunu, O., Bosserelle, C., Lane, E., 2023. Tsunami runup and inundation in Tonga from the January 2022 eruption of Hunga Volcano. Pure Appl. Geophys. 180 (1), 1–22.
Brenna, M., Cronin, S.J., Smith, I.E., Pontesilli, A., Tost, M., Barker, S., Tonga'onevai, S., Kula, T., Vaiomounga, R., 2022. Post-caldera volcanism reveals shallow priming of an intra-ocean arc andesitic caldera: Hunga volcano, Tonga, SW Pacific. Lithos 412, 106614.
Burnham, C., 1985. Energy release in subvolcanic environments; implications for breccia formation. Econ. Geol. 80 (6), 1515–1522.
Caratori Tontini, F., Bassett, D., de Ronde, C.E., Timm, C., Wysoczanski, R., 2019. Early evolution of a young back-arc basin in the Havre Trough. Nat. Geosci. 12 (10), 856–862.
Carn, S.A., Krotkov, N.A., Fisher, B.L., Li, C., 2022. Modest Volcanic SO2 Emissions During the 2021–2022 Hunga Tonga–Hunga Ha'apai Eruptions. AGU Fall Meet. Abstr. V25B–0092.
Casas, A.S., Wadsworth, F.B., Ayris, P.M., Delmelle, P., Vasseur, J., Cimarelli, C., Dingwell, D.B., 2019. SO2 scrubbing during percolation through rhyolitic volcanic domes. Geochim. Cosmochim. Acta 257, 150–162.
Cashman, K.V., Sparks, R.S.J., Blundy, J.D., 2017. Vertically extensive and unstable magmatic systems: a unified view of igneous processes. Science 355 (6331) eaag3055.
Caudron, C., Girona, T., Taisne, B., Suparjan, S., Gunawan, H., Kristianto, K., Kasbani, K., 2019. Change in seismic attenuation as a long-term precursor of gas-driven eruptions. Geology 47 (7), 632–636.
Christenson, B., Reyes, A., Young, R., Moebis, A., Sherburn, S., Cole-Baker, J., Britten, K., 2010. Cyclic processes and factors leading to phreatic eruption events: Insights from the 25 September 2007 eruption through Ruapehu Crater Lake, New Zealand. Journal of Volcanology and Geothermal Research 191 (1–2), 15–32.
Christenson, B., White, S., Britten, K., Scott, B., 2017. Hydrological evolution and chemical structure of a hyper-acidic spring-lake system on Whakaari/White Island, NZ. J. Volcanol. Geotherm. Res. 346, 180–211.
Christiansen, R.L., Peterson, D.W., Lipman, P., Mullineaux, D., 1981. Chronology of the 1980 eruptive activity. US Geol. Surv. Prof. Pap. 1250, 17–30.
Clare, M.A., Yeo, I.A., Watson, S., Wysoczanski, R., Seabrook, S., Mackay, K., Hunt, J.E., Lane, E., Talling, P.J., Pope, E., 2023. Fast and destructive density currents created by ocean-entering volcanic eruptions. Science 381 (6662), 1085–1092.
Conder, J.A., Wiens, D.A., 2006. Seismic structure beneath the Tonga arc and Lau back-arc basin determined from joint Vp, Vp/Vs tomography. Geochem. Geophys. Geosyst. 7 (3).
Cooper, L.B., Plank, T., Arculus, R.J., Hauri, E.H., Hall, P.S., Parman, S.W., 2010. High-Ca boninites from the active Tonga Arc. J. Geophys. Res. Solid Earth 115 (B10).
Cooper, L., Plank, T., Arculus, R., Hauri, E., Kelley, K.A., 2022. Arc–Backarc Exchange Along the Tonga–Lau System: Constraints From Volatile Elements. J. Petrol. 63 (8), egac072.
Cox, S.F., 2010. The application of failure mode diagrams for exploring the roles of fluid pressure and stress states in controlling styles of fracture-controlled permeability enhancement in faults and shear zones. Geofluids 10 (1–2), 217–233.
Cox, S., Knackstedt, M., Braun, J., 2001. Principles of Structural Control on Permeability and Fluid Flow in Hydrothermal Systems.
de Ronde, C.E., Hannington, M., Stoffers, P., Wright, I., Ditchburn, R., Reyes, A., Baker, E., Massoth, G., Lupton, J., Walker, S., 2005a. Evolution of a submarine magmatic-hydrothermal system: Brothers volcano, southern Kermadec arc, New Zealand. Econ. Geol. 100 (6), 1097–1133.
de Ronde, C.E., Massoth, G.J., Baker, E.T., Lupton, J.E., 2005b. Submarine hydrothermal venting related to volcanic arcs. In: Giggenbach Memorial volume, Simmons, S.F., Graham, I.G. (Eds.), Soc. Econ. Geol. and Geochem. Soc. Special Publ, 10, pp. 91–109.
de Ronde, C., Baker, E., Massoth, G., Lupton, J., Wright, I., Sparks, R., Bannister, S., Reyners, M., Walker, S., Greene, R., 2007. Submarine hydrothermal activity along the mid-Kermadec Arc, New Zealand: Large-scale effects on venting. Geochem. Geophys. Geosyst. 8 (7).
de Ronde, C.E., Massoth, G.J., Butterfield, D.A., Christenson, B.W., Ishibashi, J., Ditchburn, R.G., Hannington, M.D., Brathwaite, R.L., Lupton, J.E., Kamenetsky, V.S., 2011. Submarine hydrothermal activity and gold-rich mineralization at Brothers Volcano, Kermadec Arc, New Zealand. Mineral. Deposita 46, 541–584.
de Ronde, C., Chadwick, W., Ditchburn, R., Embley, R., Tunnicliffe, V., Baker, E., Walker, S., Ferrini, V., Merle, S., 2015. Molten sulfur lakes of intraoceanic arc volcanoes. Volcan. Lakes 261–288.
Díaz, J., Rigby, S., 2022. Energetic output of the 2022 Hunga Tonga–Hunga Ha 'apai volcanic eruption from pressure measurements. Shock Waves 32 (6), 553–561.
Donner, S., Steinberg, A., Lehr, J., Pilger, C., Hupe, P., Gaebler, P., Ross, J., Eibl, E., Heimann, S., Rebscher, D., 2023. The January 2022 Hunga Volcano explosive eruption from the multitechnological perspective of CTBT monitoring. Geophys. J. Int. 235 (1), 48–73.
Driesner, T., 2007. The system H2O–NaCl. Part II: Correlations for molar volume, enthalpy, and isobaric heat capacity from 0 to 1000° C, 0 to 5000bar, and 0 to 1 X NaCl. Geochim. Cosmochim. Acta 71 (20), 4902–4919.
Driesner, T., Heinrich, C.A., 2007. The system H 2 O–NaCl. Part I: Correlation formulae for phase relations in temperature–pressure–composition space from 0 to 1000° C, 0 to 5000bar, and 0 to 1 X NaCl. Geochim. Cosmochim. Acta 71 (20), 4880–4901.
Engelder, T., Lacazette, A., Barton, N., Stephansson, O., 1990. Natural hydraulic fracturing. In: Proceedings of the International Symposium on Rock Joints, 4-6 June at Loen, Norway, pp. 35–43.
Evan, S., Brioude, J., Rosenlof, K.H., Gao, R.-S., Portmann, R.W., Zhu, Y., Volkamer, R., Lee, C.F., Metzger, J.-M., Lamy, K., Walter, P., Alvarez, S.L., Flynn, J.H., Asher, E., Todt, M., Davis, S.M., Thornberry, T., Vömel, H., Wienhold, F.G., Stauffer, R.M., Millán, L., Santee, M.L., Froidevaux, L., Read, W.G., 2023. Rapid ozone depletion after humidification of the stratosphere by the Hunga Tonga Eruption. Science 382 (6668), eadg2551.
Ferrini, V., 2022. Bathymetry Grid of Hunga Tonga-Hunga Ha'apai Volcano Generated from Data Acquired during Falkor Cruise FK160407 (2016). IEDA.
Fischer, T.P., Chiodini, G., 2015. Volcanic, magmatic and hydrothermal gases. In: Haruldar, S. (Ed.), The Encyclopedia of Volcanoes. Elsevier, pp. 779–797.
Fischer, T.P., Morrissey, M.M., Calvache, V.M.L., Gomez, M.D., Torres, C.R., Stix, J., Williams, S.N., 1994. Correlations between SO2 flux and long-period seismicity at Galeras volcano. Nature 368 (6467), 135–137.
Giggenbach, W., 1990. The chemistry of fumarolic vapor and thermal-spring discharges from the Nevado del Ruiz volcanic-magmatic-hydrothermal system, Colombia. J. Volcanol. Geotherm. Res. 42 (1–2), 13–39.
Giggenbach, W., 1997. The origin and evolution of fluids in magmatic-hydrothermal systems. In: Barnes, H. (Ed.), Geochemistry of Hydrothermal Ore Deposits. Wiley, pp. 737–796.
Girona, T., Costa, F., Schubert, G., 2015. Degassing during quiescence as a trigger of magma ascent and volcanic eruptions. Sci. Rep. 5 (1), 18212.
Girona, T., Caudron, C., Huber, C., 2019. Origin of shallow volcanic tremor: the dynamics of gas pockets trapped beneath thin permeable media. J. Geophys. Res. Solid Earth 124 (5), 4831–4861.
Hamilton, K.M., 2023. Insights into the January 15, 2022, Hunga Eruption (Kingdom of Tonga) through Non-juvenile Pyroclasts. ResearchSpace@ Auckland.
Heap, M.J., Violay, M.E., 2021. The mechanical behaviour and failure modes of volcanic rocks: a review. Bull. Volcanol. 83 (5), 33.
Heap, M., Reuschlé, T., Farquharson, J., Baud, P., 2018. Permeability of volcanic rocks to gas and water. J. Volcanol. Geotherm. Res. 354, 29–38.
Heap, M.J., Harnett, C.E., Wadsworth, F.B., Gilg, H.A., Carbillet, L., Rosas-Carbajal, M., Komorowski, J.-C., Baud, P., Troll, V.R., Deegan, F.M., 2022. The tensile strength of hydrothermally altered volcanic rocks. J. Volcanol. Geotherm. Res. 428, 107576.
Hedenquist, J.W., Henley, R.W., 1985. Hydrothermal eruptions in the Waiotapu geothermal system, New Zealand; their origin, associated breccias, and relation to precious metal mineralization. Economic geology 80 (6), 1640–1668.
Heidarzadeh, M., Gusman, A.R., Ishibe, T., Sabeti, R., Šepić, J., 2022. Estimating the eruption-induced water displacement source of the 15 January 2022 Tonga volcanic tsunami from tsunami spectra and numerical modelling. Ocean Eng. 261, 112165.
Henley, R.W., 2015. Hyperacidic volcanic lakes, metal sinks and magmatic gas expansion in arc volcanoes. In: Volcanic Lakes. Springer, pp. 155–178.
Henley, R.W., Berger, B.R., 2011. Magmatic-vapor expansion and the formation of high-sulfidation gold deposits: Chemical controls on alteration and mineralization. Ore Geol. Rev. 39 (1), 63–74.
Henley, R.W., Berger, B.R., 2013. Nature's refineries — Metals and metalloids in arc volcanoes. Earth Sci. Rev. 125, 146–170.
Henley, R.W., Fischer, T.P., 2021. Sulfur sequestration and redox equilibria in volcanic gases. J. Volcanol. Geotherm. Res. 414, 107181.
Henley, R.W., Hughes, G.O., 2016. SO 2 flux and the thermal power of volcanic eruptions. J. Volcanol. Geotherm. Res. 190–199.
Henley, R.W., McNabb, A., 1978. Magmatic vapor plumes and ground-water interaction in porphyry copper emplacement. Econ. Geol. 73 (1), 1–20.
Henley, R.W., Seward, T.M., 2018. Gas-Solid Reactions in Arc Volcanoes; Ancient and Modern. Rev. Mineral. Geochem. 84, 309–350.
Henley, R.W., King, P.L., Wykes, J.L., Renggli, C.J., Brink, F.J., Clark, D.A., Troitzsch, U., 2015. Porphyry copper deposit formation by sub-volcanic Sulphur dioxide flux and chemisorption. Nat. Geosci. 8 (3), 210–215.
Henley, R.W., Mernagh, T., Leys, C., Troitzsch, U., Bevitt, J., Brink, F., Gardner, J., Knuefing, L., Wheeler, J., Limaye, A., 2022. Potassium silicate alteration in porphyry copper-gold deposits: a case study at the giant maar-diatreme hosted Grasberg deposit, Indonesia. J. Volcanol. Geotherm. Res. 432, 107710.
Horváth, Á., Vadas, S.L., Stephan, C.C., Buehler, S.A., 2023. One-Minute Resolution GOES-R Observations of Lamb and Gravity Waves Triggered by the Hunga Tonga-Hunga Ha'apai Eruptions on 15 January 2022. In: Authorea Preprints.
Karstens, J., Crutchley, G.J., Hansteen, T.H., Preine, J., Carey, S., Elger, J., Kühn, M., Nomikou, P., Schmid, F., Dalla Valle, G., 2023. Cascading events during the 1650 tsunamigenic eruption of Kolumbo volcano. Nat. Commun. 14 (1), 6606.

Keller, J., Gresho, M., Harris, A., Tchouvelev, A.V., 2014. What is an explosion? Int. J. Hydrog. Energy 39 (35), 20426–20433.
Kieffer, S.W., 1984. Factors Governing the Structure of Volcanic Jets. Explosive Volcanism: Inception, Evolution, and Hazards. National Academy, Washington, pp. 143–157.
Kieffer, S.W., Sturtevant, B., 1984. Laboratory studies of volcanic jets. J. Geophys. Res. Solid Earth 89 (B10), 8253–8268.
Kulichkov, S., Chunchuzov, I., Popov, O., Gorchakov, G., Mishenin, A., Perepelkin, V., Bush, G., Skorokhod, A., Vinogradov, Y.A., Semutnikova, E., 2022. Acoustic-gravity Lamb waves from the eruption of the Hunga-Tonga-Hunga-Hapai Volcano, its energy release and impact on aerosol concentrations and tsunami. Pure Appl. Geophys. 179 (5), 1533–1548.
Le Bras, R.J., Zampolli, M., Metz, D., Haralabus, G., Bittner, P., Villarroel, M., Matsumoto, H., Graham, G., Meral Özel, N., 2023. The Hunga Tonga–Hunga Ha'apai Eruption of 15 January 2022: Observations on the International Monitoring System (IMS) hydroacoustic stations and synergy with seismic and infrasound sensors. Seismol. Soc. America 94 (2A), 578–588.
Legras, B., Duchamp, C., Sellitto, P., Podglajen, A., Carboni, E., Siddans, R., Grooß, J.-U., Khaykin, S., Ploeger, F., 2022. The evolution and dynamics of the Hunga Tonga plume in the stratosphere. EGUsphere 1–19.
Lipman, P.W., 2000. Calderas. Encycloped. Volcan. 643–662.
Lloyd, J.T., 1856. Lloyd's Steamboat Directory: And Disasters of the Western Waters. JT Lloyd & Company.
Lupton, J., Lilley, M., Butterfield, D., Evans, L., Embley, R., Massoth, G., Christenson, B., Nakamura, K.I., Schmidt, M., 2008. Venting of a separate CO2-rich gas phase from submarine arc volcanoes: examples from the Mariana and Tonga-Kermadec arcs. J. Geophys. Res. Solid Earth 113 (B8).
Lynett, P., McCann, M., Zhou, Z., Renteria, W., Borrero, J., Greer, D., Fa'anunu, O., Bosserelle, C., Jaffe, B., La Selle, S., 2022. Diverse tsunamigenesis triggered by the Hunga Tonga-Hunga Ha'apai eruption. Nature 609 (7928), 728–733.
Manga, M., Fauria, K.E., Lin, C., Mitchell, S.J., Jones, M.P., Conway, C.E., Degruyter, W., Hosseini, B., Carey, R., Cahalan, R., 2018. The pumice raft-forming 2012 Havre submarine eruption was effusive. Earth Planet. Sci. Lett. 489, 49–58.
Massoth, G.J., De Ronde, C.E., Lupton, J.E., Feely, R.A., Baker, E.T., Lebon, G.T., Maenner, S.M., 2003. Chemically rich and diverse submarine hydrothermal plumes of the southern Kermadec volcanic arc (New Zealand). Geol. Soc. Lond. Spec. Publ. 219 (1), 119–139.
Matoza, R.S., Fee, D., Assink, J.D., Iezzi, A.M., Green, D.N., Kim, K., Toney, L., Lecocq, T., Krishnamoorthy, S., Lalande, J.-M., 2022. Atmospheric waves and global seismoacoustic observations of the January 2022 Hunga eruption, Tonga. Science 377 (6601), 95–100.
McNutt, S.R., 2005. Volcanic seismology. Annu. Rev. Earth Planet. Sci. 32, 461–491.
Mernagh, T.P., Leys, C., Henley, R.W., 2020. Fluid inclusion systematics in porphyry copper deposits: the super-giant Grasberg deposit, Indonesia, as a case study. Ore Geol. Rev. 103570.
Millan, L., Santee, M.L., Lambert, A., Livesey, N.J., Werner, F., Schwartz, M.J., Pumphrey, H.C., Manney, G.L., Wang, Y., Su, H., 2022. The Hunga Tonga-Hunga Ha'apai hydration of the stratosphere. Geophys. Res. Lett. 49 (13) e2022GL099381.
Newhall, C.G., Punongbayan, R., 1996. Fire and Mud: Eruptions and Lahars of Mount Pinatubo. Philippine Institute of Volcanology and Seismology Quezon City, Philippines.
NIWA-Nippon Foundation Tonga Eruption Seabed Mapping Project (TESMaP), 2023. Digital Elevation Models of Hunga Volcano, Tonga, from the MAX2201 voyage, July-August 2022 [Data set]. Zenodo. https://doi.org/10.5281/zenodo.10038898.
NOAA, 2022. Hunga Tonga-Hunga Ha'apa Volcano-generated Tsunami, Jan 15, 2022. National Oceanic and Atmospheric Administration, Pacific Marine Environmental Laboratory, NOAA Center for Tsunami Research.
Oppenheimer, C., 2011. Eruptions that Shook the World. Cambridge University Press.
Pakoksung, K., Suppasri, A., Imamura, F., 2022. The near-field tsunami generated by the 15 January 2022 eruption of the Hunga Tonga-Hunga Ha'apai volcano and its impact on Tongatapu, Tonga. Sci. Rep. 12 (1), 15187.
Phillips, W.J., 1972. Hydraulic fracturing and mineralization. J. Geol. Soc. Lond. 128 (4), 337–359.
Purkis, S.J., Ward, S.N., Fitzpatrick, N.M., Garvin, J.B., Slayback, D., Cronin, S.J., Palaseanu-Lovejoy, M., Dempsey, A., 2023. The 2022 Hunga-Tonga megatsunami: Near-field simulation of a once-in-a-century event. Sci. Adv. 9 (15), eadf5493.
Renggli, C., King, P., Henley, R., Guagliardo, P., McMorrow, L., Middleton, J., Turner, M., 2019. An experimental study of SO 2 reactions with silicate glasses and supercooled melts in the system anorthite–diopside–albite at high temperature. Contrib. Mineral. Petrol. 174 (1), 3.
Reyes, A.G., Giggenbach, W.F., Saleras, J.R., Salonga, N.D., Vergara, M.C., 1993. Petrology and geochemistry of Alto Peak, a vapor-cored hydrothermal system, Leyte Province, Philippines. Geothermics 22 (5), 479–519.
Ribo, M., Cronin, S., Stern, S., Park, S.-H., Garvin, J., Kula, T., 2023. Morphological evolution of the Hunga Tonga–Hunga Ha'apai submarine volcano after the explosive eruption. In: EGU General Assembly 2023. Copernicus Meetings, Vienna.
Ringler, A.T., Anthony, R.E., Aster, R., Taira, T., Shiro, B., Wilson, D.C., De Angelis, S., Ebeling, C., Haney, M., Matoza, R., 2023. The global seismographic network reveals atmospherically coupled normal modes excited by the 2022 Hunga Tonga eruption. Geophys. J. Int. 232 (3), 2160–2174.
Sakuno, Y., 2021. Trial of chemical composition estimation related to submarine volcano activity using discolored seawater color data obtained from GCOM-C SGLI. A case study of Nishinoshima Island, Japan, in 2020. Water 13 (8), 1100.
Sakuno, Y., Hirao, S., Taniguchi, N., 2023. Quantitatively Mapping Discolored Seawater around Submarine Volcanoes using Satellite GCOM-C SGLI Data: A Case Study of the Krakatau Eruption in Indonesia in December 2018. GeoHazards 4 (2), 107–120.
Scheu, B., Dingwell, D.B., 2022. Magma fragmentation. Rev. Mineral. Geochem. 87 (1), 767–800.
Secor, D.T., 1965. Role of fluid pressure in jointing. Am. J. Sci. 263 (8), 633–646.
Stoffers, P., Worthington, T.J., Schwarz-Schampera, U., Hannington, M.D., Massoth, G.J., Hekinian, R., Schmidt, M., Lundsten, L.J., Evans, L.J., Vaiomo'Unga, R., 2006. Submarine volcanoes and high-temperature hydrothermal venting on the Tonga arc, Southwest Pacific. Geology 34 (6), 453–456.
Tarumi, K., Yoshizawa, K., 2023. Eruption sequence of the 2022 Hunga Tonga-Hunga Ha'apai explosion from back-projection of teleseismic P waves. Earth Planet. Sci. Lett. 602, 117966.
Thiery, R., Loock, S., Mercury, L., 2010. Explosive Properties of Superheated Aqueous Solutions in Volcanic and Hydrothermal Systems, Metastable Systems Under Pressure. Springer, pp. 293–310.
Thompson, G., McNutt, S., Scruggs, M., Spera, F., Zheng, Y., Peng, Z., Yuen, D., Mandli, K., Vagasky, C., 2022. Hunga-Tonga Games: Unravelling the Timing and Size of the Biggest Volcanic Explosion in 30 Years. Authorea Preprints.
Thurin, J., Tape, C., Modrak, R., 2022. Multi-Event Explosive Seismic Source for the 2022 M w 6.3 Hunga Tonga Submarine Volcanic Eruption. Seism. Record 2 (4), 217–226.
Vergoz, J., Hupe, P., Listowski, C., Le Pichon, A., Garcés, M., Marchetti, E., Labazuy, P., Ceranna, L., Pilger, C., Gaebler, P., 2022. IMS observations of infrasound and acoustic-gravity waves produced by the January 2022 volcanic eruption of Hunga, Tonga: A global analysis. Earth Planet. Sci. Lett. 591, 117639.
Wagner, W., Kretzschmar, H.-J., 2007. International Steam Tables-Properties of Water and Steam Based on the Industrial Formulation IAPWS-IF97: Tables, Algorithms, Diagrams, and CD-ROM Electronic Steam Tables-all of the Equations of IAPWS-IF97 Including a Complete Set of Supplementary Backward Equations for Fast Calculations of Heat Cycles, Boilers, and Steam Turbines. Springer Science & Business Media.
Wagner, W., Kretzschmar, H.-J., 2008. IAPWS industrial formulation 1997 for the thermodynamic properties of water and steam. In: International Steam Tables: Properties of Water and Steam Based on the Industrial Formulation IAPWS-IF97, pp. 7–150.
Walker, S.L., de Ronde, C.E., Williams, M., Zwolak, K., Simpson, B., 2022. Ongoing Activity Within the Submarine Caldera of Hunga Tonga–Hunga Ha'apai Volcano, Tonga, Six Months After the Eruption of January 15, 2022, AGU Fall Meeting Abstracts. V16A-02.
Wright, C.J., Hindley, N.P., Alexander, M.J., Barlow, M., Hoffmann, L., Mitchell, C.N., Prata, F., Bouillon, M., Carstens, J., Clerbaux, C., 2022. Surface-to-space atmospheric waves from Hunga Tonga–Hunga Ha'apai eruption. Nature 609 (7928), 741–746.
Xu, J., Li, D., Bai, Z., Tao, M., Bian, J., 2022. Large amounts of water vapor were injected into the stratosphere by the hunga Tonga–hunga ha'apai volcano eruption. Atmosphere 13 (6), 912.
Yamaoka, K., Geshi, N., Hashimoto, T., Ingebritsen, S.E., Oikawa, T., 2016. Special issue "the phreatic eruption of Mt. Ontake volcano in 2014". Earth Planet. Space 68, 1–8.
Yuen, D.A., Scruggs, M.A., Spera, F.J., Zheng, Y., Hu, H., McNutt, S.R., Thompson, G., Mandli, K., Keller, B.R., Wei, S.S., 2022. Under the surface: Pressure-induced planetary-scale waves, volcanic lightning, and gaseous clouds caused by the submarine eruption of Hunga Tonga-Hunga Ha'apai volcano. Earthq. Res. Adv. 2 (3), 100134.
Zheng, Y., Hu, H., Spera, F.J., Scruggs, M., Thompson, G., Jin, Y., Lapen, T., McNutt, S.R., Mandli, K., Peng, Z., 2023. Episodic Magma Hammers for the 15 January 2022 Cataclysmic Eruption of Hunga Tonga-Hunga Ha'apai. Geophys. Res. Lett. 50 (8) e2023GL102763.
Zimanowski, B., Büttner, R., Dellino, P., White, J.D., Wohletz, K.H., 2015. Magma–Water Interaction and Phreatomagmatic Fragmentation, The Encyclopedia of Volcanoes. Elsevier, pp. 473–484.